1-1-2012

Adaptive Traction, Torque, and Power Control Strategies for Extended-Range Electric Vehicles

Brian Patrick Benoy

Adaptive traction, torque, and power control strategies for extended-range electric vehicles

By

Brian Patrick Benoy

A Thesis
Submitted to the Faculty of
Mississippi State University
in Partial Fulfillment of the Requirements
for the Degree of Masters of Science
in Electrical Engineering
in the Department of Electrical and Computer Engineering

Mississippi State, Mississippi

August 2012

Adaptive traction, torque, and power control strategies for extended-range electric vehicles

By

Brian Patrick Benoy

Approved:

G. Marshall Molen Professor of Electrical and Computer Engineering (Committee Chair)	Nicolas Younan Professor & Head of Electrical and Computer Engineering (Committee Member)
Raymond Winton Professor of Electrical and Computer Engineering (Committee Member)	James E. Fowler Professor of Electrical and Computer Engineering (Graduate Coordinator)

Sarah A. Rajala
Dean of the James Worth Bagley
College of Engineering

Name: Brian Patrick Benoy

Date of Degree: August 11, 2012

Institution: Mississippi State University

Major Field: Electrical Engineering

Major Professor: Dr. Marshall Molen

Title of Study: Adaptive traction, torque, and power control strategies for extended-range electric vehicles

Pages in Study: 92

Candidate for Degree of Masters of Science

Modern hybrid electric and pure electric vehicles are highly dependent on control algorithms to provide seamless safe and reliable operation under any driving condition, regardless of driver behavior. Three unique and independently operating supervisory control algorithms are introduced to improve reliability and vehicle performance on a series-hybrid electric vehicle with an all-wheel drive all-electric drivetrain. All three algorithms dynamically control or limit the amount of torque that can be delivered to the wheels through an all-electric drivetrain, consisting of two independently controlled brushless-direct current (BLDC) electric machines. Each algorithm was developed and validated following a standard iterative engineering development process which places a heavy emphasis on modeling and simulation to validate the algorithms before they are tested on the physical system. A comparison of simulated and in-vehicle test results is presented, emphasizing the importance of modeling and simulation in the design process.

Key words: hybrid electric vehicle, automotive control, traction control, torque splitting, power control

DEDICATION

I would like to dedicate this research to my parents, Warren and Sue Benoy, and my sister Laura.

ACKNOWLEDGEMENTS

The author expresses his sincere gratitude to the Mississippi State EcoCAR competition team, and the department of Electrical and Computer Engineering. Special thanks to my faculty advisor and committee chair, Dr. Marshall Molen for providing academic and professional guidance throughout the course of my studies at Mississippi State University. Expressed appreciation is also due to Mr. Jonathan Hood for his dedicated assistance in the development and validation of the power control portion of this project.

TABLE OF CONTENTS

Page

LIST OF TABLES

LIST OF FIGURES

LIST OF SYMBOLS

ABS	*Anti-lock Brake System*
APM	*Electrical Auxiliary Power Module (DC/DC converter)*
APU	*Auxiliary Power Unit (engine-generator combination)*
ATL	*Active Torque Limiting*
BCM	*Battery Control Module*
BLDC	*Brushless Direct Current*
CAN	*Controller Area Network*
EREV	*Extended Range Electric Vehicle*
ESS	*Energy Storage System*
SAE	*Society of Automotive Engineers*
ECU	*Electronic Control Unit*
HIL	*Hardware-in-the-Loop*
HVIL	*High Voltage Inter-lock Loop*
MABX	*dSPACE Micro Autobox (hybrid supervisory controller)*
I^2t	*Proportional quantity to energy spent by fuse element to clear electrical fault*
ICE	*Internal Combustion Engine*
MIL	*Model-in-the-Loop*
PCS	*Power Control System*
R_a	*Adjust Rate used in TCS*

R_r	*Recover Rate used in TCS*
S_a	*Adjust Scalar used in TCS*
S_r	*Recover Scalar used in TCS*
SIL	*Software-in-the-Loop*
TCS	*Traction Control System*

CHAPTER I

INTRODUCTION

Modern hybrid electric and pure electric vehicles are highly dependent on control algorithms to provide seamless safe and reliable operation under any driving condition, regardless of driver behavior. Due to their increasing popularity, vehicles with pure electric or blended hybrid-electric powertrains have increasingly become the topic of automotive controls research due to the fact that these complex systems present many technical challenges, as well as opportunities for advancement in fuel efficiency and energy use [1].

With regard to hybrid vehicles, it is appropriate to make a distinction between the definitions of the terms powertrain and drivetrain. A powertrain includes one or more power sources that are used to provide either mechanical or electrical power to the wheels, whereas a drivetrain only describes the components that are directly responsible for making the wheels move. Figure 1.1 describes the difference between a powertrain and a drivetrain, when referring to an all-wheel drive series hybrid-electric vehicle such as the one discussed in this thesis.

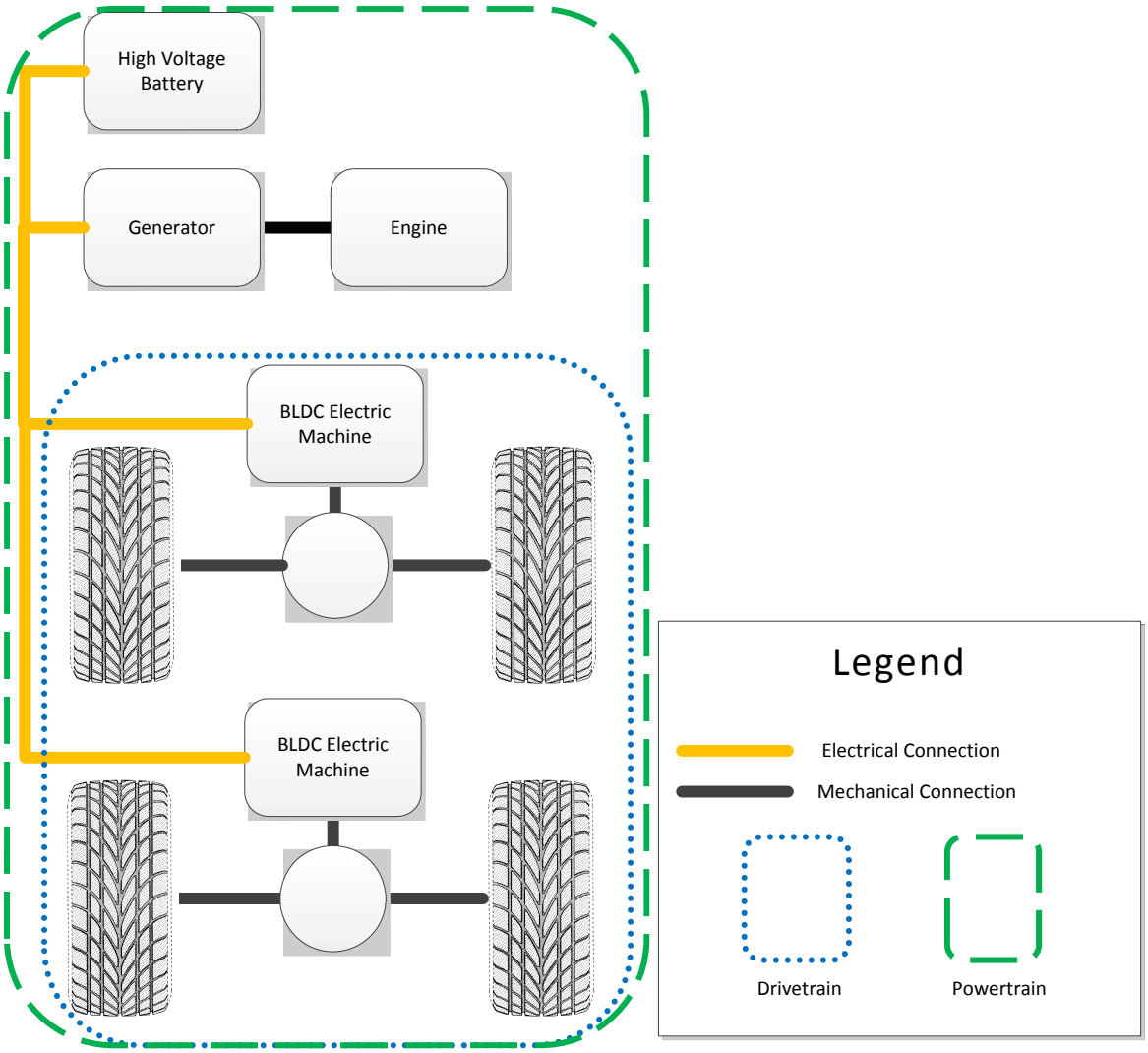

Figure 1.1 Powertrain and drivetrain diagram for an all-wheel drive series hybrid-electric vehicle.

The control algorithms presented in this thesis were developed for an all-wheel drive all-electric drivetrain, which would be appropriate for integration into a full electric or hybrid-electric vehicle platform. The all-wheel drive all-electric drivetrain for this project was designed to be part of a series hybrid-electric powertrain consisting of a diesel engine/generator combination and a 21.3 kW-hr Li-ion battery pack which provides electrical power to the electric drivetrain.

The three control algorithms that were developed for the all-wheel drive all-electric drivetrain cover three main areas of supervisory control for the system: power control, torque splitting, and traction control. Each of the algorithms operates independently from one another resulting in improved reliability and quicker integration into the main supervisory control system.

The power control algorithm was developed in order to extract the maximum amount of power during demanding driving conditions without overloading the battery pack. The torque splitting algorithm was developed to allow the vehicle to switch between efficiency and performance modes based on driver behavior. Lastly, the traction control algorithm was developed to improve vehicle performance under conditions that cause the tires to lose traction with the road surface.

Background

Electrically powered drivetrains are among the oldest types of drivetrains in the automotive industry. Electric machines have always had fewer moving parts than an internal combustion engine and typically require less maintenance. Recent advances with brushless motor technology have dramatically reduced the amount of maintenance required for electric machines while increasing their efficiency and reliability. Additionally, electric machines are much quieter and smoother than their internal combustion engine counterparts. Battery energy capacity and density have also significantly improved over the years which have made hybrid-electric and pure-electric vehicles a viable solution for low emission and fuel efficient transportation [1].

The all-wheel drive series hybrid-electric vehicle that was simulated and driven in this project was designed and built by a student team at Mississippi State University

which competed against various schools around the country in an Advanced Vehicle Technology Competition sponsored by the Department of Energy and General Motors. The series hybrid-electric architecture features independently powered all-electric front and rear drivelines. The front driveline is driven by a high performance 125-kW BLDC electric motor and is coupled to a 6.81:1 fixed gear transaxle to provide torque to the front wheels. The rear driveline is driven by a 145-kW BLDC electric motor and is coupled to a 6.67:1 locking differential to provide torque to the rear wheels. The electric drivetrain is powered from two sources. The main electrical power source is a 21.3 kW-hr lithium-ion phosphate battery pack. A 75 kW BLDC electric motor coupled to a 1.3 L turbo-diesel engine provides extended range functionality when the battery is depleted or if the vehicle is placed in a performance mode. Figure 1.2 illustrates the series hybrid-electric powertrain, as designed, on the EcoCAR platform.

Figure 1.2 EcoCAR vehicle powertrain architecture.

Figure 1.3 shows the completed vehicle, after the hybrid powertrain has been integrated into the vehicle.

Figure 1.3 Fully assembled vehicle.

The drivetrain of this vehicle was designed with performance in mind. The drive motors were selected to have significant torque at low speeds to improve acceleration performance; however, the resulting combined maximum electric power capability of the two drive motors is 70 kW more than the Li-Ion battery can supply on its own. Operating the engine/generator system can provide an additional 75 kW of electrical power for a short time, however, only 45 kW can be provided continuously, thus creating a power deficiency between the Energy Storage System (ESS) and the electric motors. The overall goal of a series hybrid-electric vehicle architecture is to use the onboard battery as much as possible to displace petroleum fuel that would otherwise be used by operating the engine. This equates to using the engine as little as possible during vehicle operation.

To meet this goal, the vehicle has two normal driving operational modes: Charge Deplete (CD) and Charge Sustain (CS). The CD operational mode requires that the ESS

(without the additional power from the engine-generator) supply all of the energy to drive the vehicle until the ESS reaches a pre-determined State of Charge (SOC). Once the ESS has reached the specified SOC, the vehicle switches to a CS operational mode. The CS mode runs the engine at a constant load (thus constant power) in order to maintain the ESS SOC within a set of limits.

Power Control (Energy Management)

There are many power control algorithms for hybrid-electric vehicles that exist in the industry today. Many focus on improving efficiency through dc/dc converter control [2] or sizing components based on drive cycle and peak power requirements [3].

Much work has been done in the area of energy management with combined ultra-capacitor and battery ESSs. Although the Extended Range Electric Vehicle(EREV) hybrid architecture studied in this thesis does not utilize an ultra-capacitor bank as a means of reducing voltage fluctuations resulting from the state of charge changing on the battery, the control theory still provides valuable insight into the methods for forecasting power based on driver input and current ESS capabilities. An energy management system of particular interest was developed by Lei Wang. This system utilizes a forecast control architecture to estimate the amount of future energy usage based on driver input and calculating available energy using system variables and an optimization equation [3]. One of the goals of the energy management strategy was to minimize energy loss due to voltage fluctuations on the battery by applying the forecast method to the control of a dc/dc converter which would stabilize the voltage on the bus with the use of an ultra-capacitor bank. The reduction of transients on the battery in turn reduces the energy

losses due to transient cycling. This strategy was of particular interest for this project because it described a method for predicting energy usage based on driver input.

Rajkumar Copparapu proposed a new method for sizing hybrid components based on force instead of peak power requirements [2]. This research was particularly informational because the power control system that was developed by the MSU researchers for the competition vehicle had to be based on the drive motor control variable, torque (force around a moment arm). In order for the power control algorithm to be effective, a relationship had to be developed between the torque control variable and estimated electrical power that would be used at the requested torque. This relationship enabled the electrical power request of the drive motor to be compared against the maximum electrical power available in the ESS. The method proposed by Copparapu could have been used in the initial component selection process to determine whether or not the size of the ESS that was selected would be sufficient in constant force situations (such as acceleration and braking).

Traction Control

Traction control systems have been thoroughly investigated for conventional vehicles for many decades. Modern vehicles use traction control to improve dynamic stability and safety of the vehicle. Keeping the tires from slipping on the road during acceleration can have performance benefits as well. The complexity of these systems depends on the design of the drivetrain. Examples of traction control systems include air intake/fuel injection modification [10], and active control of limited slip differentials [14].

Continued research has been conducted in the traction control arena due to the increase in hybrid vehicle development. Since many hybrid vehicle architectures utilize electric motors to provide either some or all of the tractive torque to the wheels, advanced traction control systems have been developed that exploit the unique torque and response characteristics of electric motors [11].

Jianlong Zhang successfully developed a fuzzy logic controller to improve the torque oscillations during a traction control event when compared to a traditional logic-based traction control system [4]. The method of developing the fuzzy controller resulted in a control system that produced targeted brake forces from the electric motor by using the negative torque capability of the drive motor. This method is very similar to a traction control system (TCS) in a conventional vehicle where the TCS is interfaced with the anti-lock brake system (ABS) whereby the ABS applies targeted brake forces on the wheels experiencing a loss of traction [1].

Dejun Yin *et al.* developed an entirely new method for traction control known as Maximum Transmissible Torque Estimation (MTTE) [11]. This method does not depend on a calculated vehicle velocity or a slip ratio derived from a complicated wheel slip algorithm based on tire and vehicle specific parameters as with conventional systems. The resulting TCS that was developed proved to be a cost effective solution to mitigating wheel slip without the need for additional sensors and customized algorithms. Dejun's method estimates the maximum transmissible torque in real time for a given electric drivetrain, which then feeds into a controller to develop a constrained torque that can be applied to the wheels. The TCS that was developed for this thesis is based on a very similar method of torque control that actively modifies the torque request based on relative motor speeds during a loss of traction.

Tire-Road Frictional Modeling

Modeling tire slip (and thus reduced friction on road surfaces) has also become an important factor for rapidly developing and testing traction control systems. Many models utilize various versions of Pacejka's Magic Formula to estimate tire slip whereby the slip ratio is determined from experimental data used to create the Magic Formula [5-7]. Unfortunately, the Magic Formula depends on a known frictional coefficient of the tire or road as well as many parameters derived from the composition and design of the rubber tire under test; thus making it difficult to simulate without the known parameters.

Sojoodi proposed a method for observing adhesion coefficient and linear velocity of a vehicle based solely on the angular velocity of the wheel [8]. This method was of particular interest for the development of the TCS because the method did not require a slip ratio nor did it depend on Pacejka's Magic Formula. The method was designed to be a real-time information source for other controllers in a vehicle, but it could also be used for plant modeling purposes. This method was studied for model development during this project but not implemented on the Hardware In the Loop (HIL) simulator for real-time control development due to the complexity of the model. However, Sojoodi did present the goal of detecting wheel slip using angular velocity, which was an idea that was incorporated into the TCS design for this thesis.

Since developing a simple traction control system is only one of several tasks for the supervisory control development project, a basic model needed to be developed to simulate the tire-road frictional coefficient varying over time (thus creating tire slip that can be detected by the TCS). To solve this problem in a timely fashion, a unique method for modeling a variable frictional coefficient was developed (Appendix C) and validated in this thesis.

Torque Splitting

The unique design of the AWD drivetrain for the series hybrid-electric vehicle in this project allows for independent control of front and rear drive motors. Kang proposes a vehicle control algorithm that determines torque assignments to the front and rear drive motors as well as clamp forces for all four brake calipers based on a conglomerate of inputs including yaw, roll, acceleration, deceleration, and various tire parameters [9]. This paper was the only work known to this author that included research on the same type of independently controlled electric drivetrain that was designed and integrated on the vehicle for this project. As a result, Kang's work was very useful for determining the constraints and limits of design with the project vehicle. There are several notable differences between the control algorithms presented by Kang and the ones presented in this thesis; namely the fact that the PCS, TCS and torque splitting algorithms presented in this thesis are completely isolated from the functionality of the mechanical brakes. Another difference is the modularity of the control systems. The control architecture presented by Kang includes high level and low level control algorithms that depend on each other to properly operate. The control architecture presented in this thesis (which is described in much more detail in Chapter II) is of a modular nature which improves the robustness of the overall control architecture by isolating the systems from each other.

CHAPTER II

CONTROL STRATEGIES

The three control algorithms that were developed for the all-wheel drive all-electric drivetrain cover three main areas of supervisory control for the system: power control, torque splitting, and traction control. Each of the algorithms operates independently from one another, allowing for improved reliability and quicker integration into the main supervisory control system.

The power control algorithm was developed in order to extract the maximum amount of power during demanding driving conditions without overloading the battery pack. The torque splitting algorithm was developed to allow the vehicle to switch between efficiency and performance modes based on driver behavior. Lastly, the traction control algorithm was developed to improve vehicle performance under conditions that cause the tires to lose traction with the road surface. Figure 2.1 illustrates the three control algorithms and how they are implemented in the supervisory controls. The power control algorithm is encompassed by the blue rectangle, torque splitting is captured by the red box, and traction control is highlighted by the green box.

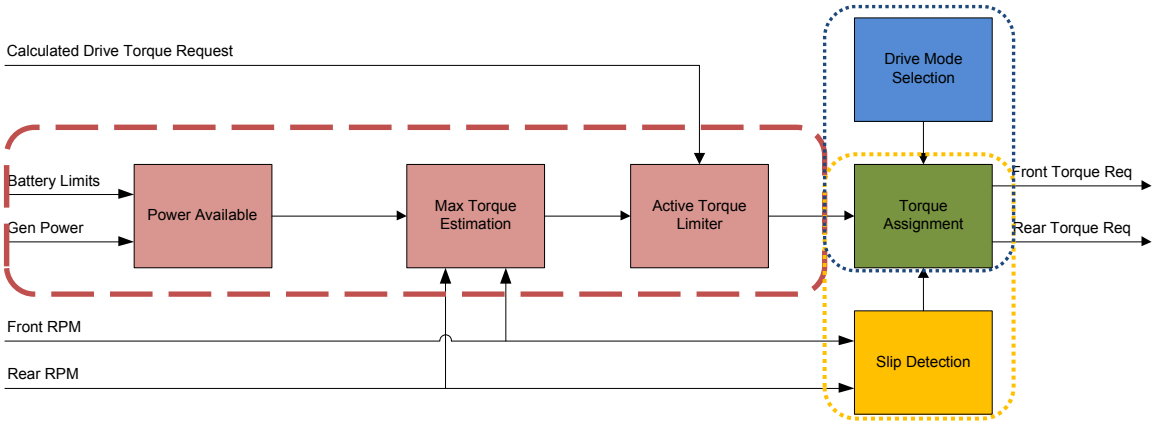

Figure 2.1 High-level diagram of power, torque splitting, and traction control algorithms.

Power Control

It was determined that the two electric drive motors that were selected for the all-wheel drive all-electric drivetrain have the capability to use 70 kW more electrical power than the lithium ion battery pack could deliver without assistance from the engine. Since the engine must also be started using energy from the high voltage battery, it became clear that the battery cannot supply enough power to start the engine during a deep discharge. This is because the electric machines in the drivetrain are already using all the electrical power from the battery during a deep discharge. The inability to start the engine (and thus provide supplemental electrical power from the generator) during a deep discharge, in turn, meant that the drive motors can and will use more electrical power than is available from the battery alone. As a result, a control algorithm had to be developed to allow the engine to start under any condition, as well as force the drive motors to adhere to the maximum electrical power limits of the battery pack (not the electrical power limits of the drive motors) by dynamically limiting the amount of torque that could be requested.

The algorithm operates based on power available, which is a combination of the battery's allowed discharge/charge power limits and the engine/generator's electrical contribution to the system. Since most power control systems are component specific, detailed information about some of the components is restricted for proprietary reasons.

Controller Design

The power control system (PCS) was designed to have three distinct modular stages: power available, maximum torque estimation, and active torque limiting. The modular design allows for concise and organized data flow, which in turn simplified the debugging process during the algorithm development phase. Figure 2.2 shows this modular design.

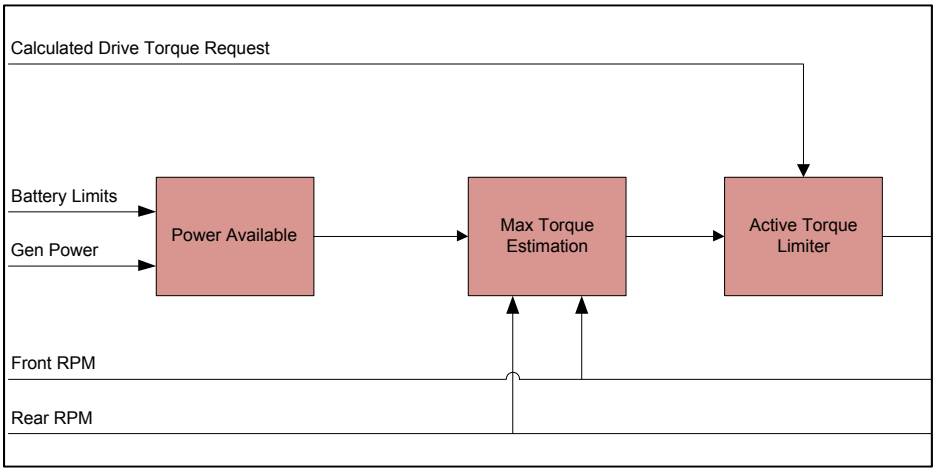

Figure 2.2 Three-stage power control architecture.

Power Available

The power available section calculates the amount of electrical power that the ESS can supply at any given time, including when the generator is adding power to the system, as seen in Fig. 2.2. The specific limits and details about how the limits are

calculated for the battery are based on proprietary information. The maximum battery power is then summed with the power being generated by the generator to produce a total system power that is available to the drive motors.

Maximum Torque Estimation

The max torque estimation section calculates the maximum torque that can be applied to each motor based on available power and motor speed. Since the front and rear motors are different sizes, the front motor uses 46% of the available power, and the rear uses the remaining 54%. The torque estimation is calculated using a 3-dimensional surface map that was empirically derived using dynamometer test data. Each surface map matches the motor manufacturers published limits for the specific motor.

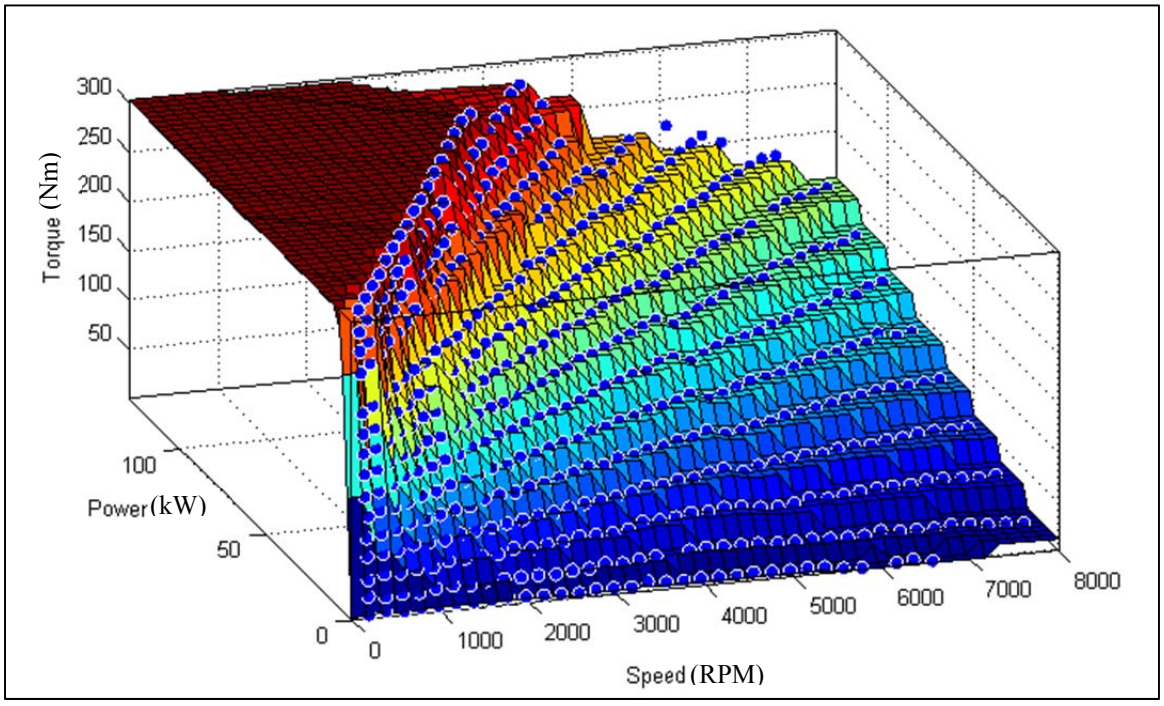

Figure 2.3 Torque estimation plot for 125 kW BLDC electric drive motor.

Active Torque Limiting

The active torque limiting (ATL) section is the last section of the PCS and is comprised of a classic state machine that matches the driver's torque request to the maximum available torque from the max torque prediction section of the architecture. The ATL state machine is absolutely necessary to force the driver's torque request to fall within the capabilities of the electrical system. In fact, it is the most important piece of the entire vehicle's power control strategy because it controls exactly how much torque (and thus power) can be commanded from the traction motors.

It was experimentally found that the Battery Control Module (BCM) that controls the battery pack does allow for the battery to be overpowered for short durations without determining that an Emergency Power Off (EPO) condition has occurred. When an EPO condition does occur, the BCM commands the bus contactors inside the pack to interrupt the circuit between the high voltage bus and the battery pack which in turn disables the vehicle, even if the vehicle is moving. In an effort to prevent an EPO condition and at the same time maximize the amount of usable energy that can be extracted from the battery during deep discharges, the ATL system was developed with three parameters that can be adjusted to fine-tune the reaction time and performance of the power control algorithm while remaining within the limits of the BCM. The three parameters are overload time, rate adjust, and restore time.

The overload time parameter forces the ATL state machine to wait a specified time to begin limiting torque after an overload condition has been detected, thus creating an overpower condition. This parameter works in conjunction with the rate adjust parameter to control how much energy is used while the overload condition is present.

The rate adjust parameter allows for the decay rate of the active limiting system to be modified, thus scaling the amount of energy present in the overload condition. The "rate adjust" and "overload time" parameters determine the *area* of the overload region on a graph of power usage as shown in Fig. 2.4. The area of the overload region is also directly related to the BCM limit known as the "software I^2t limit".

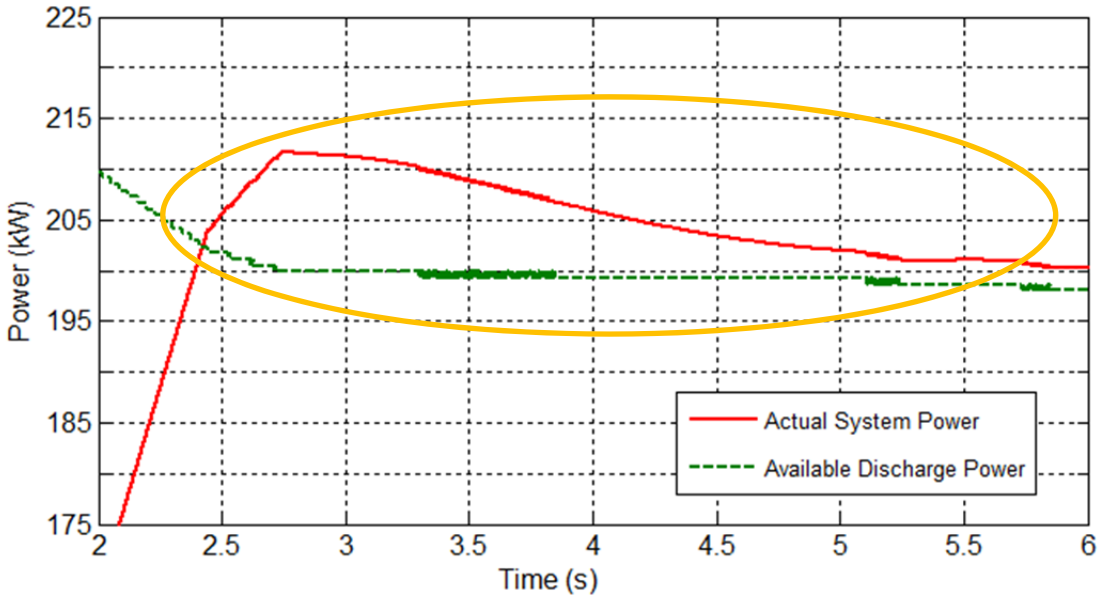

Figure 2.4 Overload region identified during active power limiting.

The restore time parameter allows for an adjustable amount of time that the active limiting system will wait before allowing another overload event to occur. This time period is determined by the amount of thermal heat that is generated during charge or discharge and the subsequent time that is required to pass before another overload event can occur. The specific amount of time that the battery pack must wait is a known parameter to the BCM but is considered proprietary to the battery manufacturer, thus it had to be experimentally determined. This parameter is also related to the "software I^2t

limit" inside the BCM. As shown in Fig. 2.5, the "restore time" parameter determines how frequently an overload event can occur.

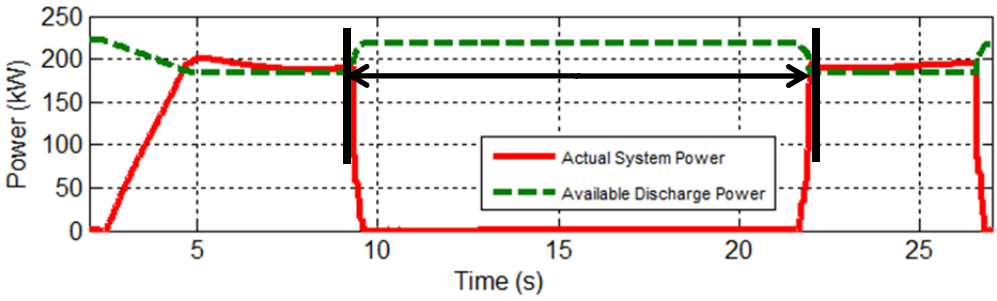

Figure 2.5 Restore time identified between overload events shown in brackets.

Active Torque Limiting State Machine

The ATL state machine has four distinct states: normal operation, over-limit, apply limit, and under-limit. Figure 2.6 gives a graphical representation of the active limiting state machine.

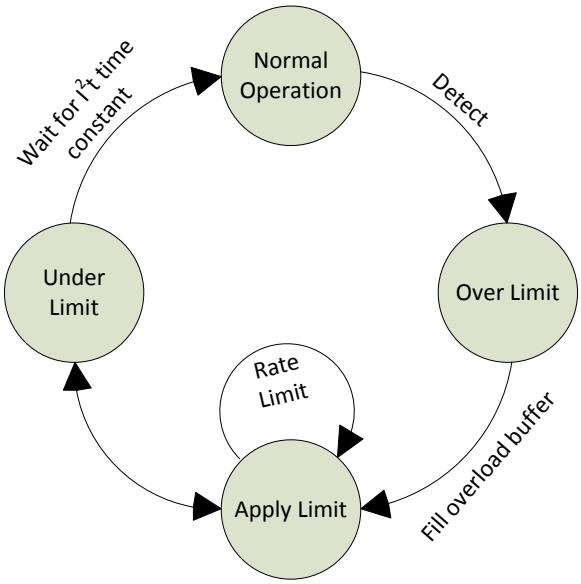

Figure 2.6 Active limiting state machine.

The ATL state machine initializes, and usually operates in the normal operation state. The normal operation state allows the requested torque to pass through as allowed torque whenever the driver is not requesting more than the maximum available torque.

When the ATL detects that the driver has requested more torque than the calculated maximum available torque, the over limit state is entered. The state machine then fills the overload buffer (or waits for the overload time to pass) before moving to the apply limit state.

The apply limit state matches the driver requested torque to the calculated maximum available torque by determining a torque limit using the equation:

$$T_o = \begin{cases} T_o' - \left|\frac{T_o' - T_{mx}}{2}\right|, & T_o \geq T_{mx} \\ T_o' + \left|\frac{T_o' - T_{mx}}{2}\right|, & T_o < T_{mx} \end{cases} \tag{2.1}$$

where:

T_o is limited torque output
T_o' is limited torque output from previous time step
T_{req} is driver torque request
T_{mx} is maximum torque available

The two cases in Eq. 2.1 are similar, but they are both necessary in order for the torque limit to follow the curve of the maximum torque available.

The apply limit state constantly checks both the limited torque and the driver's torque request against the maximum available torque and determines which direction to adjust the limited torque. It is important to note that the power control strategy never circumvents the driver's torque request; it only modifies the request when it determines that the system cannot meet the drivers' request. The limited torque output of the state machine is constantly adjusted in this state as long as the limited torque is still above the maximum available torque. The rate of the adjustment of the limited torque output (and

thus the rate of the system's power usage) is determined by the previously defined parameter "rate adjust". If the limited torque output or the drivers' torque request falls below the maximum available torque, the active limiting state is exited and the state machine moves on to the Under Limit state.

The under-limit state passes through driver torque request as allowed torque as long as the driver request is under the limit. The active limiting state will reactivate if the driver request is more than or equal to half of the maximum available torque. The under-limit state features another tunable parameter, restore time, which dictates how long the driver must request less than half of the maximum available torque before an over power region of active limiting can be accessed. The restore time is based on maximum discharge energy of the battery and I^2t constraints dictated by the battery controller.

Since the drive motors have the capability of generating power during braking, an identical active limiting state machine was developed to match driver braking torque to the maximum available braking torque. It was decided that two independent state machines would be more reliable and less complex than one state machine that handled all power states.

Torque Splitting

The uniquely independent all-wheel drive (AWD) design of the test vehicle provided the opportunity to develop equally unique torque splitting algorithms to improve or alter performance, drive quality, or energy efficiency. Table 2.1 shows the various torque splitting strategies that were developed and highlights the ones that were eventually implemented on the vehicle.

Table 2.1 Experimental torque splitting strategies

Torque Split Strategy	Description	Comments
Front-Bleed Rear	Front motor receives torque request first, rear motor receives remaining torque request, if any exists.	Implemented on vehicle for efficiency
Rear-Bleed Front	Rear motor receives torque request first, front motor receives remaining torque request, if any exists.	Bad drive quality due to rear motor mount design
Equal Motor % Split	Each motor receives an equal percentage of their maximum capable torque.	Implemented on vehicle for performance driving
10/90 Front/Rear Torque	Total torque available split between front & rear motor	Implemented as a limp-home mode
20/80 Front/Rear Torque	Same as above	Bad drive quality due to rear motor mount design
30/70 Front/Rear Torque	Same as above	Underperformed compared to Equal % Motor Split
40/60 Front/Rear Torque	Same as above	Same as above
50/50 Front/Rear Torque	Same as above	Same as above
60/40 Front/Rear Torque	Same as above	Good drive quality, high energy usage
70/30 Front/Rear Torque	Same as above	Same as above
80/20 Front/Rear Torque	Same as above	Same as above
90/10 Front/Rear Torque	Same as above	Implemented on vehicle as a limp-home mode

After eliminating several torque splitting schemes based on qualitative analysis, others were chosen to be researched to improve drive quality, overall driveline efficiency, and performance. Driveline efficiency and performance were specifically addressed in the selected torque splitting strategies as these had the best drive quality results.

Controller Design

The front and rear traction motors operate in significantly different efficiency zones at constant vehicle speeds. This is due in part to the fact that the front and rear drive motors have different power and torque capabilities. Since the rear motor is more powerful than the front motor, it has a different peak efficiency zone. Additionally, the front gear ratio of 6.81:1 is slightly larger than the rear ratio of 6.67:1 that was selected. The different gear ratios ultimately translate to different motor speeds at the same vehicle speed. As a result, the efficiency zones can be changed by adjusting the amount of driver requested torque that is sent to each motor.

The selected "front-bleed-rear" torque splitting strategy was developed to maximize the efficiencies of the combined drivelines. The front-bleed-rear strategy requests torque from the front motor first. If the front motor cannot fulfill all of the requested torque, the remaining torque request is then sent to the rear motor, as shown:

$$T_{front} = \begin{cases} T_{req}, & T_{req} < 300 \\ 300, & T_{req} \geq 300 \end{cases} \tag{2.2}$$

$$T_{rear} = \begin{cases} 0, & T_{req} < 300 \\ T_{req} - T_{front}, & T_{req} \geq 300 \end{cases} \tag{2.3}$$

Where:
T_{front} is front motor request
T_{rear} is rear motor request
T_{req} is driver request

For this particular vehicle, the front motor has a maximum torque of 300 Nm while the rear motor has a maximum torque of 400 Nm. The sum of the front and rear maximum torques results in a maximum of 700 Nm that the driver can request at low speeds. Equations 2.2 and 2.3 show how the limits of the front motor determine the request for the rear.

The vast majority of torque requests during normal driving are within the operating range of the front motor, which means that the rear motor is used very infrequently under normal driving conditions. By operating the front motor more often in a higher torque region, it was hypothesized that the vehicle's energy efficiency would increase. Simulation results are presented in Chapter IV that support this hypothesis.

During simulation, it was noted that performance characteristics such as acceleration and handling were negatively affected by the front-bleed-rear strategy when compared to a constant torque split between the front and rear motors. To address this issue, a performance mode was developed to switch the torque splitting to an equal motor percentage split when the system detects aggressive driver behavior. The method for calculating each motor's contribution to the overall requested torque is shown by a simple proportional calculation:

$$T_{front} = \frac{T_{fmx}}{T_{total}} * T_{req} \tag{2.4}$$

$$T_{rear} = \frac{T_{rmx}}{T_{total}} * T_{req} \tag{2.5}$$

where

T_{fmx} is maximum front motor torque
T_{rmx} is maximum rear motor torque
T_{total} is the sum of front and rear maximum torques
T_{req} is driver torque request

The system automatically switches back to the front-bleed-rear strategy after a specified time and the aggressive driver behavior is no longer present. The effects of changing the torque splitting strategy from an efficiency mode to a performance mode are discussed in Chapter IV.

Traction Control

To address tire slip in the test vehicle, a traction control system was developed that detects when tires are slipping and mitigates the slippage by reducing torque request. The system also re-applies the torque at a reduced rate when slippage is determined to maximize acceleration under low traction conditions. If the tires continue to slip, the system will continuously adjust torque to find the maximum torque that can be applied without slippage. Although the same methods can be applied to anti-lock braking (ABS) systems, traction control is not anti-lock braking. Traction control, in this context is purely intended to maximize vehicle stability and control during acceleration and deceleration in reduced traction environments, whereas ABS only functions during deceleration.

Controller Design

The test vehicle was designed to have independently controlled front and rear single-speed gear ratio reduction drivelines driven by BLDC electric machines. As a result, two identical and independent traction control systems were developed. Similar to the power control strategy, the traction control strategy is designed to be modular for a clear and logical flow of information, which simplifies the debugging process. The two stages are: slip detection and mitigation.

Slip Detection & Vehicle Speed Calculation

The slip detection system has two methods of detection: relative and absolute speed and acceleration comparisons. The relative speed comparison method provides the Traction Control System (TCS) with individually calculated front and rear vehicle velocities in units of miles per hour (mph), based off of the front and rear BLDC motor

speeds. The two velocities are compared with each other, and the TCS is activated if the difference exceeds a threshold. The individually calculated front and rear vehicle speeds enable the TCS to accurately determine the correct vehicle speed during a loss of traction. Equations 2.6 and 2.7 give the method that was developed for calculating the front and rear vehicle speeds:

$$v_f = \frac{2\pi \cdot r_d \cdot N_f}{g_f} \tag{2.6}$$

$$v_r = \frac{2\pi \cdot r_d \cdot N_r}{g_r} \tag{2.7}$$

Where:

r_d is wheel radius
v_f is front velocity
g_f is front motor gear ratio
N_f is front motor RPM
v_r is rear velocity
g_r is rear motor gear ratio
N_r is rear motor RPM

Table 2.2 shows the logic behind the relative slip detection algorithm. In summary, the slip detection algorithm determines if the difference of the calculated front and rear velocities are outside of a pre-defined threshold of five miles-per-hour. The algorithm then determines (based on which motor is outside of the tolerance) whether or not to enable the respective traction control algorithm. For example, if the front velocity is 50 MPH while the rear velocity is 10 MPH, the slip detection algorithm determines that the front velocity is invalid and activates the front traction control algorithm. The slip detection algorithm also sets front and rear slip active (SA) bits which are used by the mitigation state machine discussed in the next section.

The speed validity signal was developed to identify whether or not the algorithms that are used to calculate vehicle speed are accurate. Speed validity is lost whenever both

the front and rear motor experience slippage. Without the use of accelerometers in combination with a Global Positioning System (GPS), it is very difficult to determine actual vehicle speed if all of the wheels are slipping. Since external information was not available for this project, vehicle speed when all wheels are slipping was calculated simply as the average of both the front and the rear calculated vehicle speeds as shown in Eqs.6 and 7. A truth table was developed to determine the most accurate vehicle speed given different wheel slip conditions:

Table 2.2 Traction Control Enable and Vehicle Speed Truth Table

Front Wheel Slip Detected?	Rear Wheel Slip Detected?	Speed Valid	Speed Calculation
false	false	true	Use Average Speed
false	true	true	Use Front Speed
true	false	true	Use Rear Speed
true	true	false	Use Average Speed

The front and rear slip values are determined by the slip detection algorithm as previously mentioned by comparing the difference of the front and rear velocities against a threshold value. This novel and simple method was developed to provide the driver with a vehicle speed that was as accurate as possible, even if traction control is active.

The slip detection and vehicle speed calculation algorithm controls the mitigation portion of the TCS by enabling and disabling the active management of driver torque request.

Mitigation

The mitigation portion of the traction control system is designed to override individual front and rear motor torque requests when tire slip is detected by the upstream slip detection portion of the algorithm. It is also the last stage the driver's torque request must pass through before the request is sent to the motor over the vehicle's Controller Area Network (CAN). The original mitigation section of the traction control system is a state machine with six states as shown in Fig.2.7.

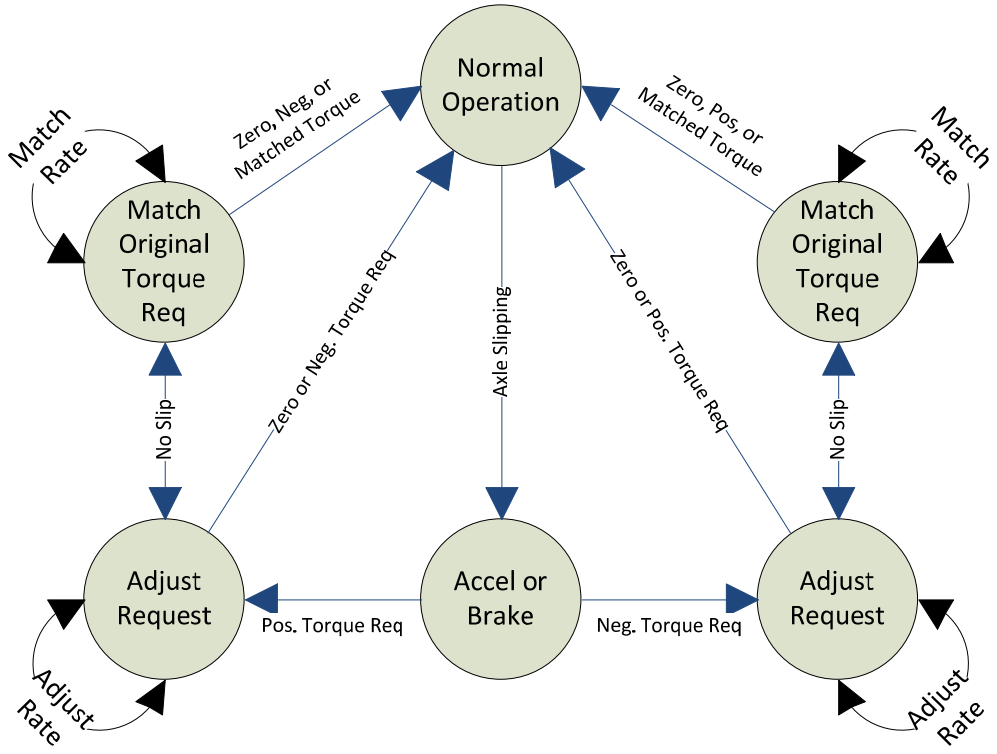

Figure 2.7 Mitigation state machine for traction control system.

Once wheel slip is detected, the mitigation strategy first determines if the driver is requesting positive (traction) or negative (braking) torque. If the driver is requesting traction torque, the system sets a Traction Control Active flag that is visible to the rest of

the supervisory control strategy and begins to de-rate the torque until one of two cases is met:

- the driver request is less than the current adjusted torque
- motor slip is no longer detected

The torque request de-rating and subsequent matching are determined by:

$$T_o = \begin{cases} S_a * T_o', & SA = 1 \\ T_o' + S_r, & SA = 0 \end{cases} \tag{2.8}$$

where:

T_o is torque request output to the motor
T_o' is torque request output from the previous time step
SA is slip active bit
S_a is adjust scalar
S_r is recover scalar

It is important to note that the output torque request is always matched to the driver request when slip is not active. When the mitigation system is active, the driver torque request is latched as the ceiling value of torque. The TCS then modifies the torque request with the S_a parameter until slip is no longer detected. As soon as slip is no longer detected, the TCS attempts to match the latched torque value by modifying the output torque request with the S_r parameter. The TCS will attempt to match the latched value of torque until either the system meets the requested torque or the driver requests less than the output torque request. The driver request is constantly monitored to ensure that the mitigation state machine is not modifying the torque request outside of the limits that the driver has placed on the system. The resulting output of the activated traction control system is shown in Fig. 2.8.

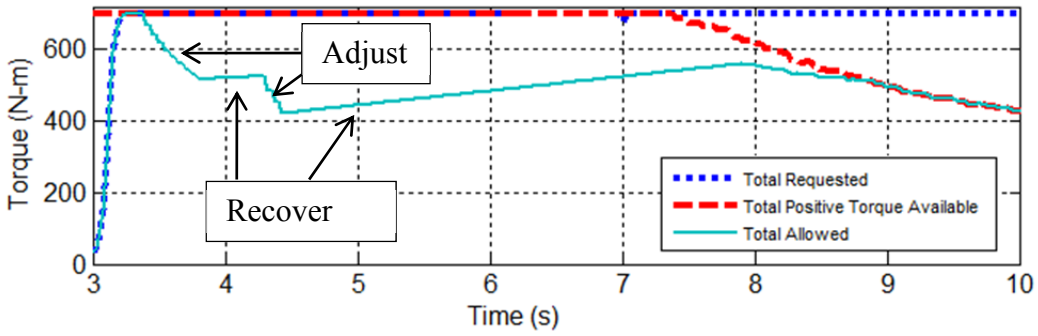

Figure 2.8 Resulting torque request during an active traction control event.

The series of events is executed in the opposite order in the event that slip is detected during braking. It is important to note that due to a competition requirement preventing modification of ABS, the original TCS was modified to only function during acceleration. Figure 2.9 shows the implemented TCS, with the deceleration portion of the mitigation algorithm disabled.

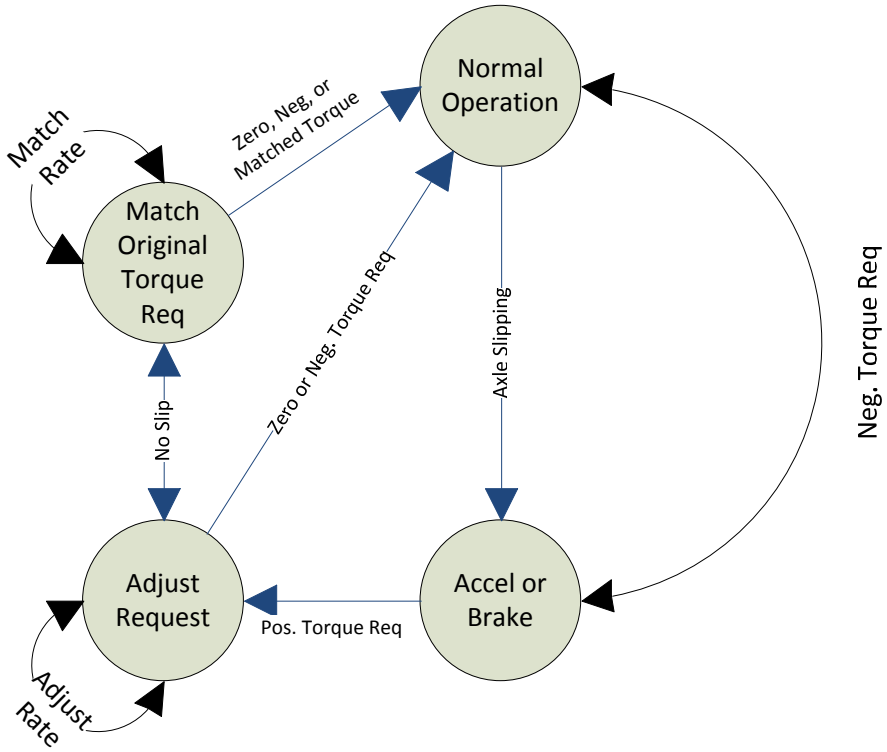

Figure 2.9 Implemented mitigation state machine for Traction Control System.

Traction control system performance during deceleration was not modeled on the HIL or in-vehicle because functionality during braking was outside of the scope of the project.

The TCS is a simple, yet effective means of mitigating a loss of traction on a fixed gear reduction electric drivetrain. The ability to independently control the traction of both the front and rear drivelines enables the vehicle to apply torque to the motor with traction while actively mitigating slip on the driveline experiencing slip. Although the functionality of the traction control system is strictly passive (torque is reduced from an original request), this feature forms the basis of a torque-vectoring system which could not only decrease torque from the slipping motor but also add the equal and opposite amount of reduced torque to the motor with traction. A system of clutches in the differential would then apply the most torque to the wheel with the most traction.

CHAPTER III

VALIDATION METHODOLOGY

Algorithm validation was performed in several steps following the standard "V-diagram" product development cycle. Validation is essential with control systems. Making a small change in one section of a control system has the potential to expose a flaw in another portion of the control system, which can have a catastrophic effect on system stability or safety. The V-diagram is one the most common methods of validation because of the modular approach: unit, subsystem, system, and acceptance.

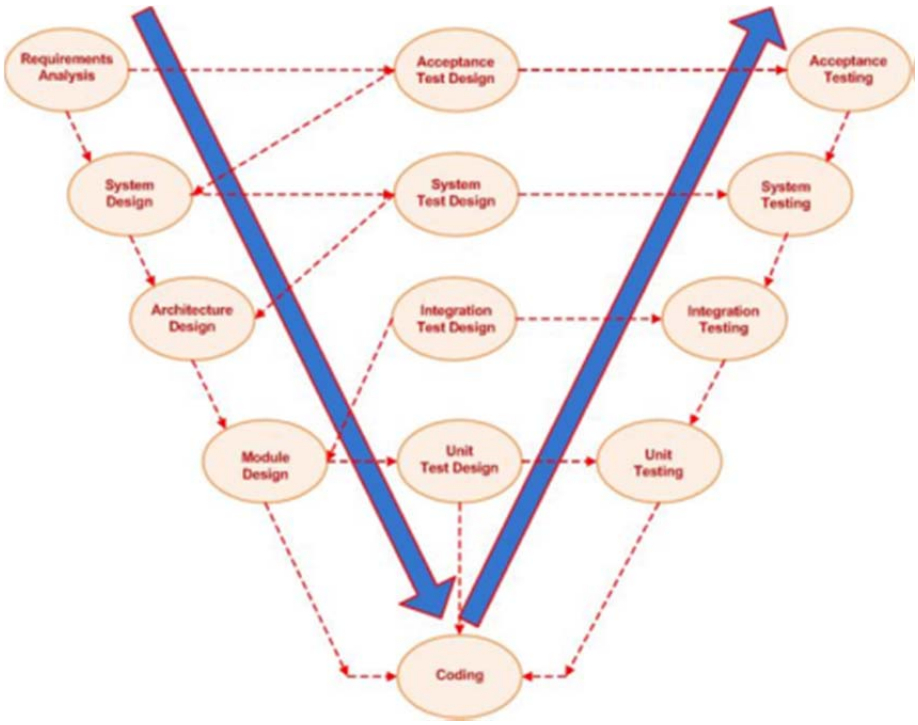

Figure 3.1 V-diagram for software development.

Following the V-diagram forces the development process to begin and revert back to the smallest portion of a control system, known as the unit, or module. Initial controller validation always starts with offline unit testing. The unit, or module, is then incrementally integrated into a system level test environment where more than multiple modules work together based on feedback from other systems and modules. Closed loop controller testing using plant models instead of real physical systems is known as In-the Loop testing. This method of testing has three forms: Model in the Loop (MIL), Software In-the Loop (SIL), and Hardware In-the Loop (HIL). Each stage increases in complexity as the controller testing progresses.

Offline Unit Testing

The new algorithm is developed in an open loop environment by deriving test procedures from Design Failure Mode Effects and Analysis (DFMEA) that test the basic functionality and fault detection of the new algorithm. After the new module is validated in the open-loop environment, the module is then integrated into the controller on a system level. Once the integration step is complete, the development moves to closed loop offline and online validation testing.

Model In-the Loop Testing

Model In the Loop (MIL) is the farthest removed from the real world and is the first stage in closed-loop controller development. This method of testing is for validation of high level controller architectures and testing basic functionality of system components. It is intended to be used for vehicle architecture selection where specific details about component/controller interactions are not necessary. All data flow is in engineering units, and all components assume ideal operation. The benefit of all data

flow being in engineering units is that the conversions to physical signals that communicate to other systems such as analog voltages, PWM, or serial communication do not exist. This allows for a simpler controller design and less complex interface to the plant model. An example of MIL is Argonne National Laboratory's Powertrain Systems Analysis Toolkit (PSAT) and Autonomie simulation tools, which allow for quick component replacement with minimal redesign of the basic control functions [13]. PSAT was used to select the hybrid architecture for the test vehicle in this investigation.

Software In-the Loop (SIL) System Testing

SIL is used to integrate test response times and any combination of faults identified through Design Failure Mode and Effects Analysis (DFMEA) or Fault Tree Analysis (FTA) into the validation process. SIL is much more complex than MIL and requires specific signals related to the components that are being simulated. Simulations can be run in various configurations depending on the requirements of the test. Short time length, high fidelity simulations can use variable step size computation, whereas real time target compilation can simulate communication network failures or inter-system harmonics. SIL is the first closed loop testing where the tested code should be identical to production code in that it incorporates communication delays, conversion resolutions, and other factors that add to the complexity of physical control system integration.

Hardware In-the Loop (HIL) Real-Time Testing

Hardware In-the Loop simulation integrates the physical controller and sensors into the simulation environment. A HIL chassis simulator contains a real time processor that controls various I/O boards that allow the engineer to physically connect controllers and sensors to the chassis exactly like they would be connected in a real vehicle. HIL

chassis simulators also allow for automated electrical fault insertion, which is extremely helpful for diagnostic detection. For this controller development, the HIL has been used for everything from fault insertion to endurance testing. It allows the controller to push the limits of the components without the risk of damaging the physical components or system. Automated test procedures have been developed for regression testing purposes. HIL also validates controller I/O to ensure that the scaling between engineering units and electrical signals is done properly and accurately. This is the last step of validation before the new controller algorithm is tested in a real vehicle. The HIL setup that was used for this project is shown in Fig. 3.2.

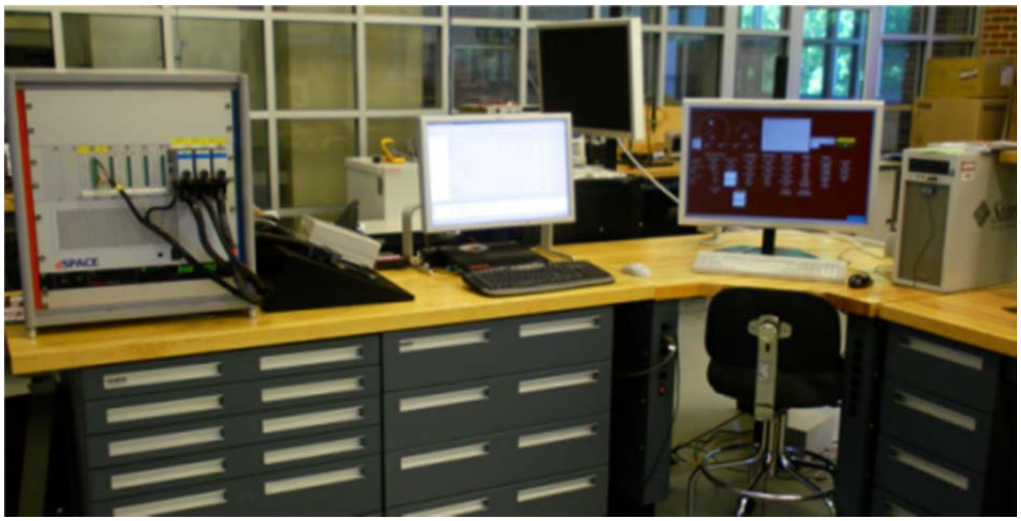

Figure 3.2 HIL setup

The HIL was used extensively throughout the entire controller development process, and was vital to the success of the project.

In-Vehicle Validation

The final stage of validation for a new control algorithm is in-vehicle acceptance tests. This is either done on a closed course or on a chassis dynamometer, depending on

the test requirements. For example, a traction control system cannot be tested on a chassis dynamometer because the road surface coefficient of friction cannot be changed. Figures 3.3 and 3.4 show actual in-vehicle testing that was performed on the vehicle.

Figure 3.3 Dynamic vehicle testing at General Motor's Milford proving grounds.

Figure 3.4 Traction control testing on a closed road track in Starkville, MS.

Figure 3.5 Chassis dynamometer testing at Center for Advanced Vehicular Systems (CAVS) in Starkville, MS.

Test Procedures

Several standardized tests were performed throughout the development process in order to capture both simulated and real-world performance results of the implemented strategies. Table 3.1 below contains short descriptions of each standard test that was performed at each stage of the development process.

Table 3.2 Standardized experiments to be performed for offline, SIL, HIL, and In-Vehicle test platforms.

Test	Description
WOT 0-60 dry surface	Torque Request ramps from 0-700 Nm and remains there until 60mph is attained
WOT 50-70 dry surface	Torque Request ramps from 0-700 Nm when vehicle is at 50mph
70-0 @ 10% travel	Torque Request ramps to whatever 10% brake pedal is and stays there until 0 mph
Braking 70 @ 50% travel	Torque Request ramps to whatever 50% brake pedal is and stays there until 0 mph
Wet-dry surface WOT w/o TC	Torque Request ramps from 0-700 Nm and remains there until 60mph is attained
Wet-dry surface WOT w/ TC	Torque Request ramps from 0-700 Nm and remains there until 60mph is attained
WOT no power limiting	Torque Request ramps from 0-700 Nm and remains there until 60mph is attained

A more complete description of the tests summarized in Table 3.1 can be found in Appendix A.

CHAPTER IV

PERFORMANCE RESULTS

Validation results were obtained by performing the standardized tests defined in Chapter III on three testing platforms: SIL, HIL, and in-vehicle. These results were separated into the same groups as they were developed: Power Control, Torque Splitting, and Traction Control. Wide-open throttle (WOT), Modified WOT, and regenerative braking tests were executed on all test platforms and for each control strategy. Each control strategy was independently enabled and disabled in order to compare the functionality of the control system under test. Table 4.1 defines a validation matrix that was developed to verify that each of the control strategies under development was tested on each test platform. The entries identified in Table 4.1 as unavailable correspond to either the dynamometer being unavailable or safety concerns regarding the performance of that specific test.

Table 4.1 Validation matrix, with non-applicable sections noted.

Control Algorithm	SIL	HIL	In-Vehicle
Power Control (disabled)			Unavailable
Power Control (enabled)			
Torque Splitting (disabled)			Unavailable
Torque Splitting (enabled)			
Traction Control (disabled)			
Traction Control (enabled)			

In order to analyze the performance of each control algorithm independently, each standardized test generated a series of four graphs to be analyzed. The tests were

performed once with the algorithm under test disabled and again with the algorithm under test enabled. The results are then compared against each other to validate the effectiveness of the control strategy. Table 4.2 describes the graphs that were generated for each test that was performed.

Table 4.2 Description and purpose of graphs

Graph Title	Purpose
Vehicle Speed and Pedals	Validate driver inputs to the control system under test
Power Limits	Validate total system power used is within the system power min/max limits
Capable vs. Allowed: Torque	Validate individual front and rear torque requests when compared to min/max limits
Capable vs. Allowed: Power	Validate individual front and rear power requests when compared to min/max limits

Although the test validation consisted of following the standard process of SIL to HIL to in-vehicle testing, only HIL test results are presented here because of the extensive volume of data that was collected. The SIL and in-vehicle test results from this project can be found in Appendix D and E, respectively.

Power Control

HIL testing validated the response time and stability of the controller strategy design in a real-time environment on the physical controller hardware. Standardized WOT and braking tests were performed on the HIL simulator as described in Appendix A. Figure 4.1 shows the vehicle speed and pedal positions for the WOT HIL test.

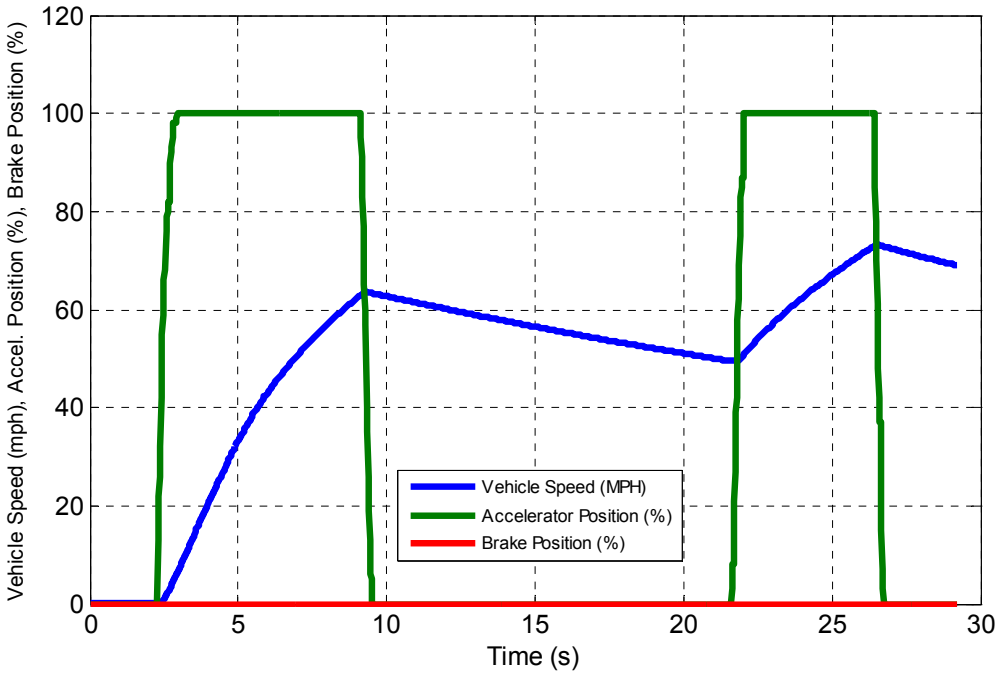

Figure 4.1 Vehicle speed and pedal positions for WOT test on HIL.

Figure 4.2 illustrates the available system power verses actual power used with power control enabled.

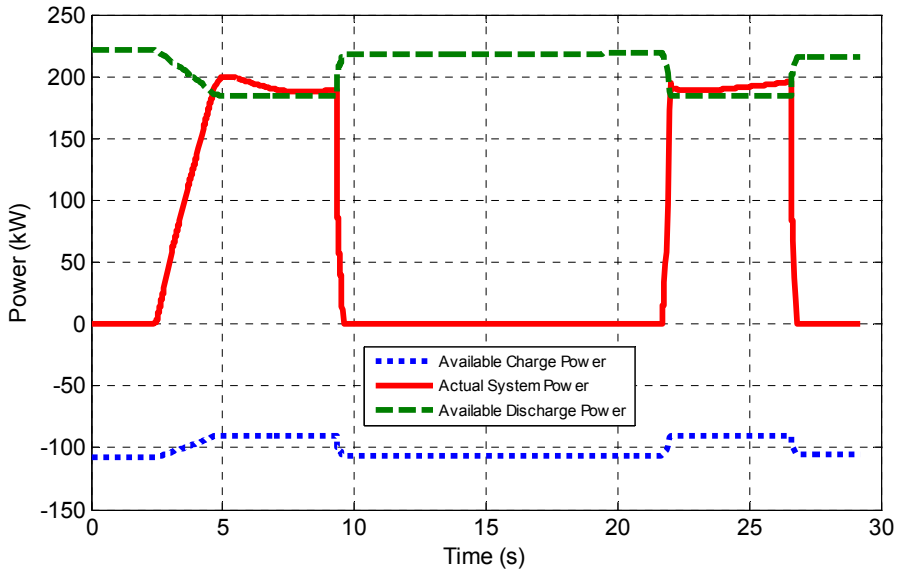

Figure 4.2 Total available system power and actual system power during WOT test on HIL.

Note that the actual power exceeds the power limits of the battery for a short period of time. The limit may temporarily be exceeded as long as the I^2t limit established by the battery controller is maintained. Figures 4.3 and 4.4 show the performance characteristics of each of the motors with power control enabled.

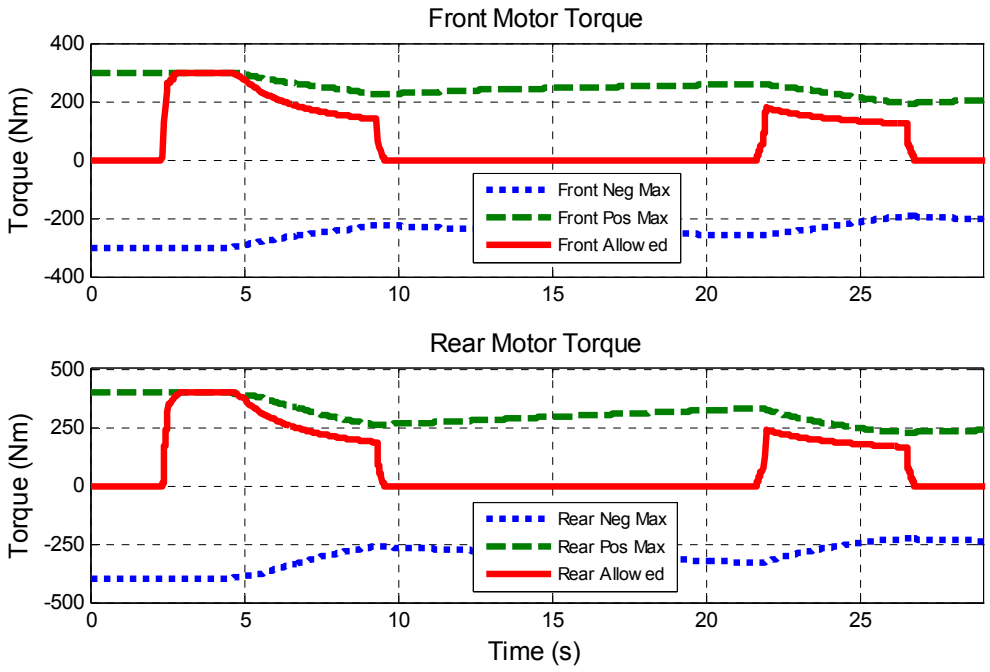

Figure 4.3 Torque comparison between motor limits and torque requested with power control enabled during WOT.

It is important to note that the torque command for both motors follows the same general shape as the motor limits, but the command is scaled to match the power available from the battery. Figure 4.4 illustrates the power limits and actual power used from each drive motor.

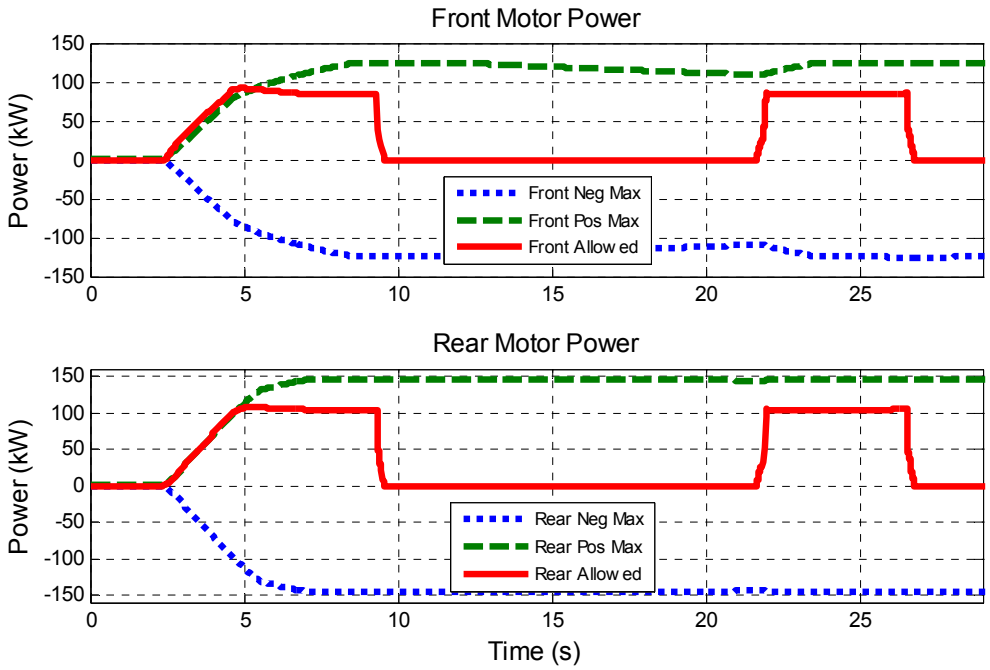

Figure 4.4 Power comparison between motor limits and actual power used with power control active during WOT.

The regenerative braking test was performed with the vehicle coasting to 70 miles per hour, and the brake pedal being applied to 50% travel until the vehicle comes to a complete stop. Figure 4.5 illustrates the pedal position inputs and the resulting vehicle speed for the regenerative braking test.

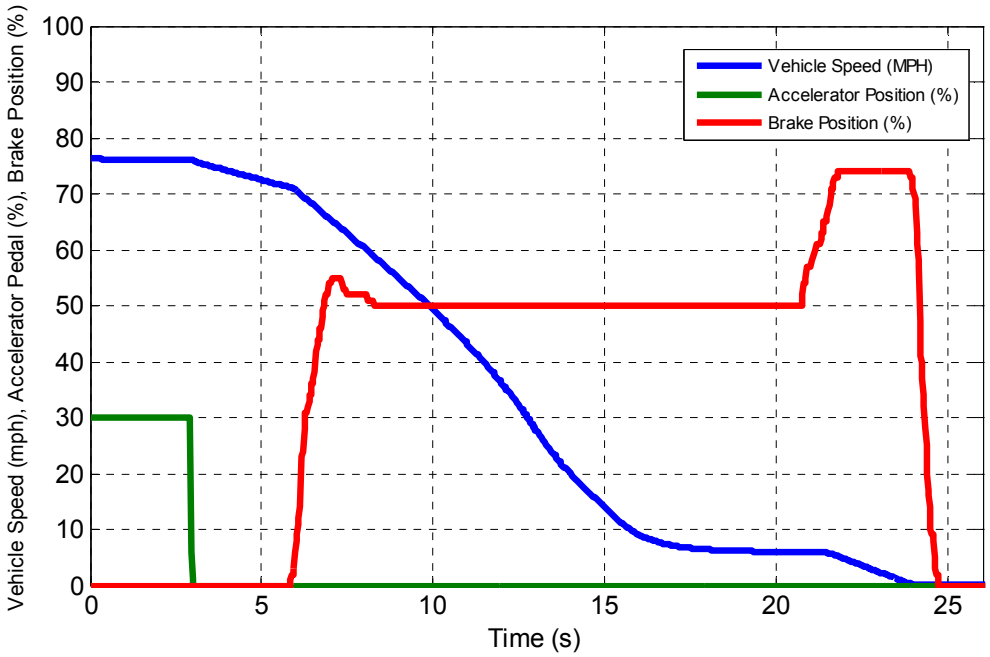

Figure 4.5 Pedal positions and resulting vehicle speed for regenerative braking test on HIL.

Note that the brake pedal is pressed to around 75% at low vehicle speeds. This is due to the fact that the regenerative braking is set to fade out at low speeds, which requires the brake to be pressed further to engage the mechanical brakes.

Figures 4.6-4.8 show the performance characteristics of the power control system during the same regenerative braking event as Fig. 4.5 depicts. Figure 4.6 illustrates the power control strategy limiting the total power going into the battery pack during regenerative braking.

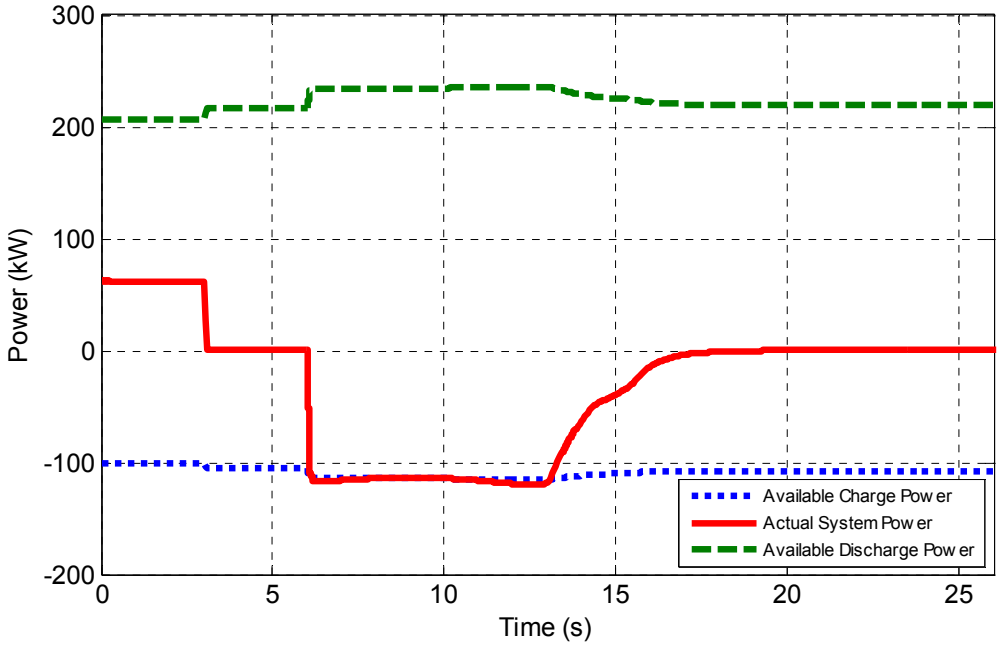

Figure 4.6 Total available system power and actual power generated during regenerative braking on HIL. Braking starts at approximately 6 s.

Figure 4.7 splits the braking event into the front and rear motors, which allows for a closer look at the torque available verses the torque commanded during braking.

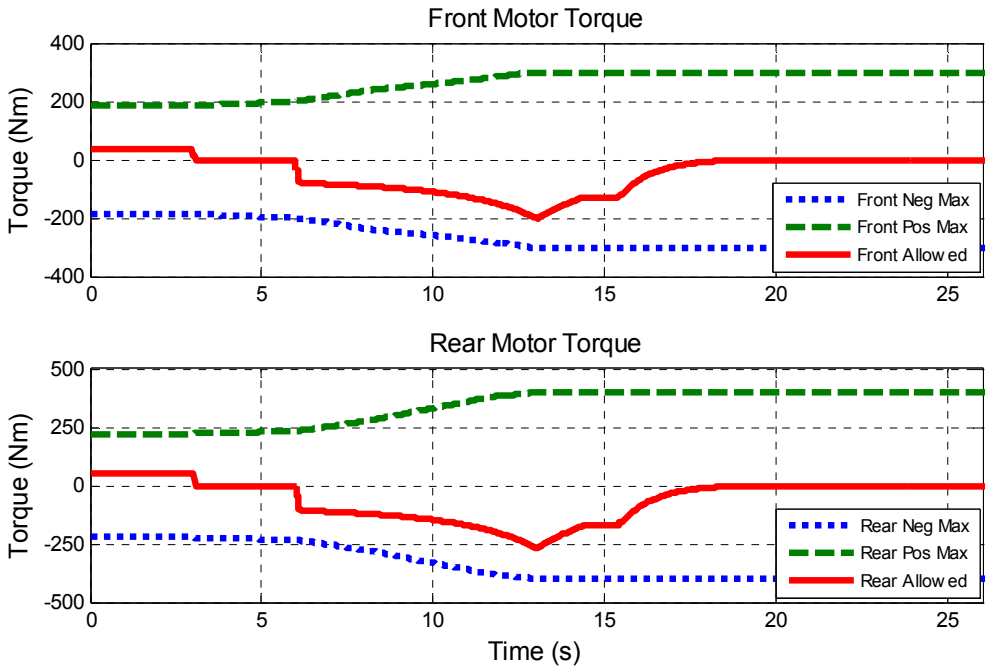

Figure 4.7 Torque comparison between motor limits and torque requested with power control enabled during regenerative braking.

The HIL simulation produces a commanded torque curve that approximately follows the same curve as the motor's limit, except it is scaled to match the battery's power limit. Figure 4.8 shows how the limited torque command results in a limited power generation from each of the motors during the same braking event.

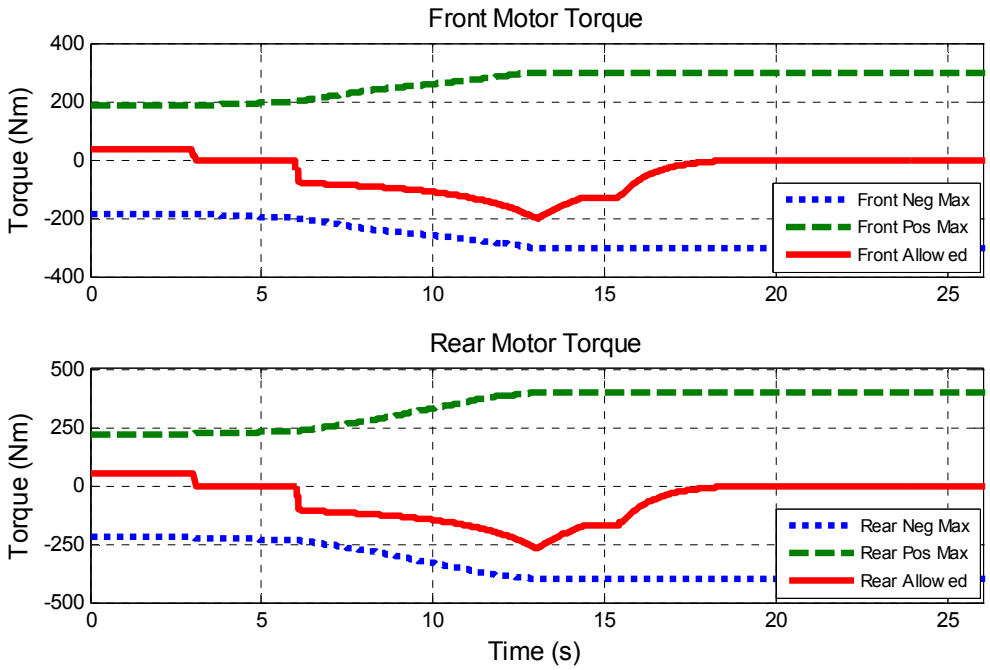

Figure 4.8 Power comparison between motor limits and actual power used with power control active during regenerative braking.

HIL simulations allowed the power limiting control strategy to be refined from a proof of concept design to a fully functional control strategy. After extensive SIL and HIL validation testing, the power limiting strategy was integrated into the in-vehicle hybrid supervisory controller to begin in-vehicle testing. The results of the in-vehicle testing can be found in Appendix E

Torque Splitting

The following figures compare the efficiencies of the front and rear motors throughout a combined urban and highway drive cycle HIL simulation with various torque splitting strategies enabled.

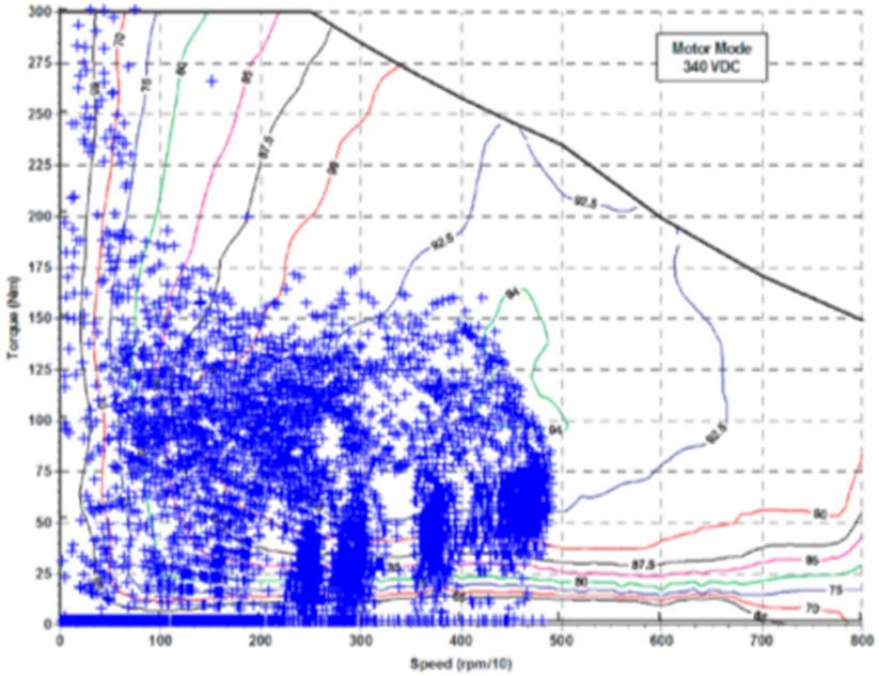

Figure 4.9 Front-Bleed-Rear torque split strategy implemented (front motor).

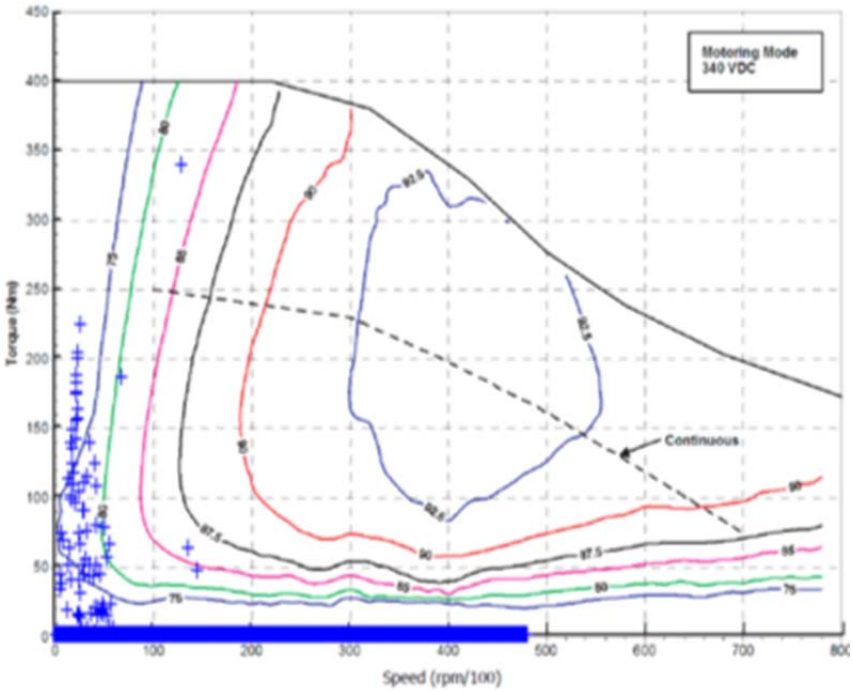

Figure 4.10 Front-Bleed-Rear torque split strategy implemented (rear motor).

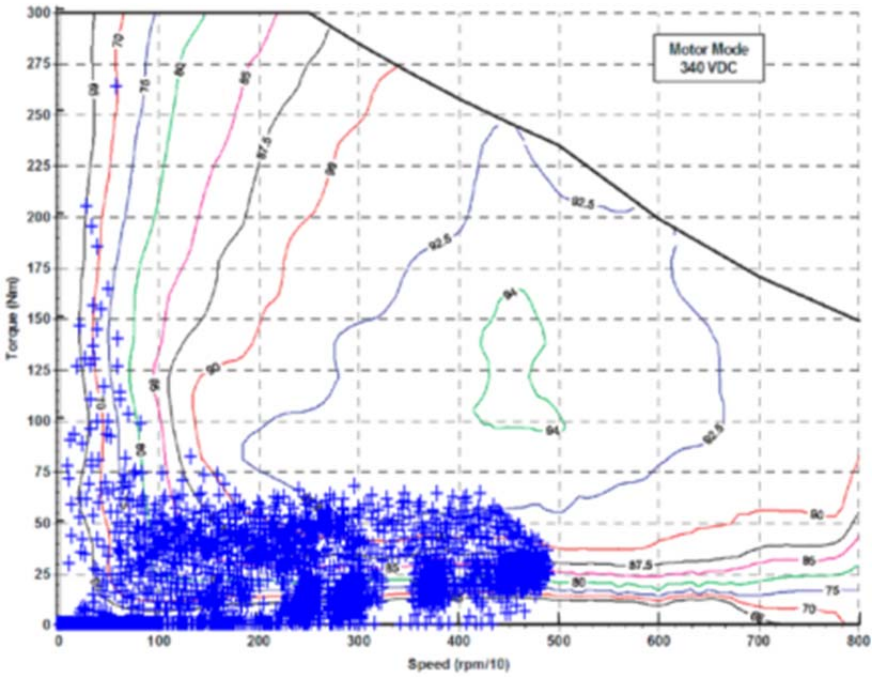

Figure 4.11 46/54 Front Rear torque split strategy implemented (front motor).

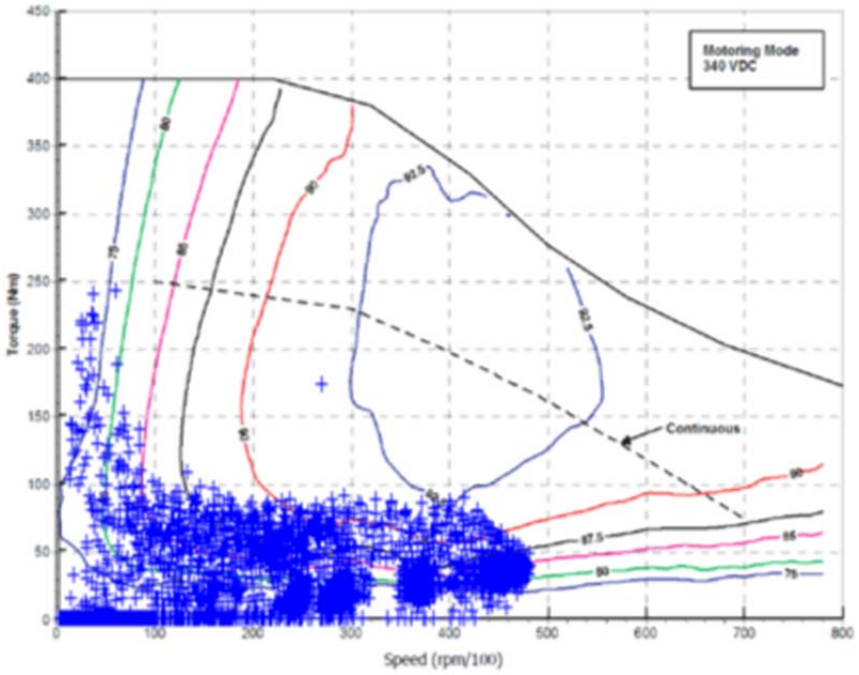

Figure 4.12 46/54 Front Rear torque split strategy implemented (rear motor).

A summary of the analysis of the drive cycle data (shown in Table 4.3) with front-bleed-rear and 46/54 split gives a clear distinction between the two torque splitting strategies.

Table 4.3 Analysis of drive motor efficiency data taken during combined urban and highway drive cycle simulations.

Torque Split Strategy	Avg Front Motor Efficiency	Avg Rear Motor Efficiency	Percentage of Use (Front/Rear)	Total Overall Motor Efficiency
Front-Bleed Rear	87.5	72.2	98.9/1.1	87.3
46/54	72.9	76.9	N/A	76.2

The front-bleed-rear torque split strategy also showed some performance decreases due to the initial longitudinal and normal forces acting on the tires during WOT take-off.

Table 4.4 Analysis of different torque split strategies during WOT acceleration event.

Torque Split Strategy	0-60 MPH Time (seconds)	50-70 MPH Time (seconds)
Front-Bleed Rear	5.9	3.5
46/54	5.6	2.8

The addition of the performance mode allows the vehicle to operate efficiently when the driver wants efficiency without sacrificing performance when it is needed. Since the performance mode is a passive control strategy, the mode exits to the default efficiency mode under several conditions:

- After an aggressive driving timer expires
- Any time the vehicle leaves a “normal” operating mode as a result of a fault or malfunction

- The vehicle is turned off

The torque splitting strategy effectively allows the vehicle to achieve high performance marks when performance is needed and high efficiency numbers when efficiency is needed, as Tables 4.3 & 4.4 describe. Production vehicles utilize toggle switches that the driver can operate in order to switch the vehicle into different operating modes, but these types of switches (also known as an active control strategy) were strictly forbidden for the competition that the test vehicle was designed for. As a result, the torque splitting strategy was designed to be passive; requiring no extra input from the driver other than normal driving actions such as pedal control and steering inputs.

Traction Control

As described in Chapter III, the traction control system contains relative and absolute algorithms for detecting wheel slip. The traction control HIL test results were largely dependent on the model that was created to simulate a loss of traction at the tires. The model had several vehicle dynamics variables that were held constant that are not actually constant in real life, such as suspension spring and damping forces, as well as lateral vehicle forces. Taking those factors into account, the traction control test was designed to specifically validate the slip detection and mitigation portions of the traction control system both in the HIL and in-vehicle environments.

The HIL simulation began by placing all four tires in a reduced traction environment. WOT was then applied, and the vehicle transitioned out of the reduced traction zone. Figure 4.11 served as the baseline for the traction control validation testing activities. As intended, both the front and rear motor speeds spike initially when the tires begin to slip. As the front wheels enter the transition zone (and the coefficient of surface friction begins to rise), the tires begin to catch the ground, thus lowering the motor speed.

As the rear wheels enter the transition zone, the rear motor slows to closely match the front motor speed. It should be noted that the front and rear motor speeds are not equal due to the different drive ratios associated with each axle. It can also be seen that although both of the motors have the same maximum RPM limit imposed by the motor controllers, the rear motor reaches the maximum RPM limit, while the front motor does not.

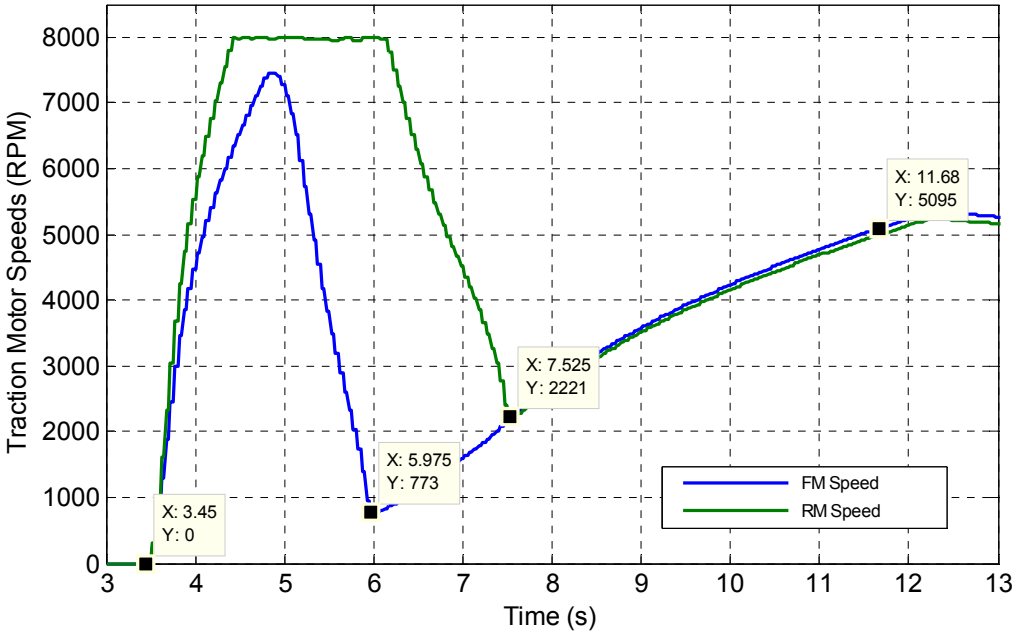

Figure 4.13 HIL simulation of WOT test with reduced traction and no traction control.

The TCS included several tuning variables, which were varied in order to tune the response time of the system. As described in Chapter II, the S_r, S_a, R_r and R_a parameters determine the waveform of the driver's torque request reduction and subsequent matching during an active traction control event. The S_a and S_r variables were fixed to 0.9 and 1, respectively, in order to prevent the introduction of harsh torque changes in the driveline during Traction Control events. The fixed S_a and S_r parameters ensure a smooth

feel on the driveline when torque is removed and added by the Traction Control System. Since the S_a and S_r parameters were fixed for consumer acceptability, the only parameters that could be changed were the rates (R_a and R_r). A quick comparison between Fig. 4.11 and Fig. 4.12 shows that the R_r of 10 ms is not effective at reducing the amount of time that the wheels are slipping. This is because the S_r parameter is relatively low. Applying Eq. 8, an interval of 10 ms with S_r equal to 1 Nm increases the matching torque by one Nm every time the TCS completes one cycle. Adjusting the rate of the matching torque can, in effect, shorten the amount of time the TCS takes to give control back to the driver.

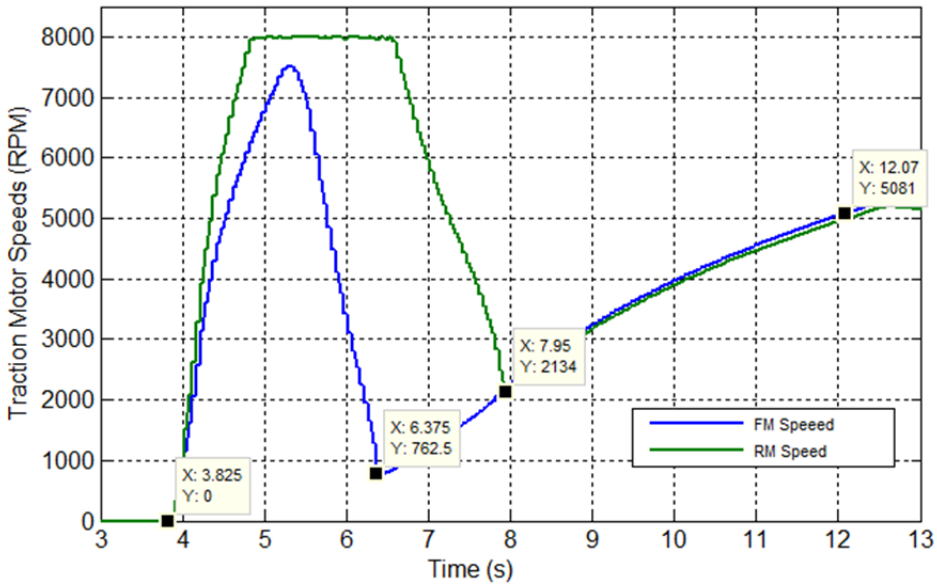

Figure 4.14 Front and rear speeds during reduced traction WOT HIL test, with R_r set to 10 ms.

Figure 4.13 shows that R_r of 5 ms reduces the amount of time that the rear tires are spinning by almost a full second.

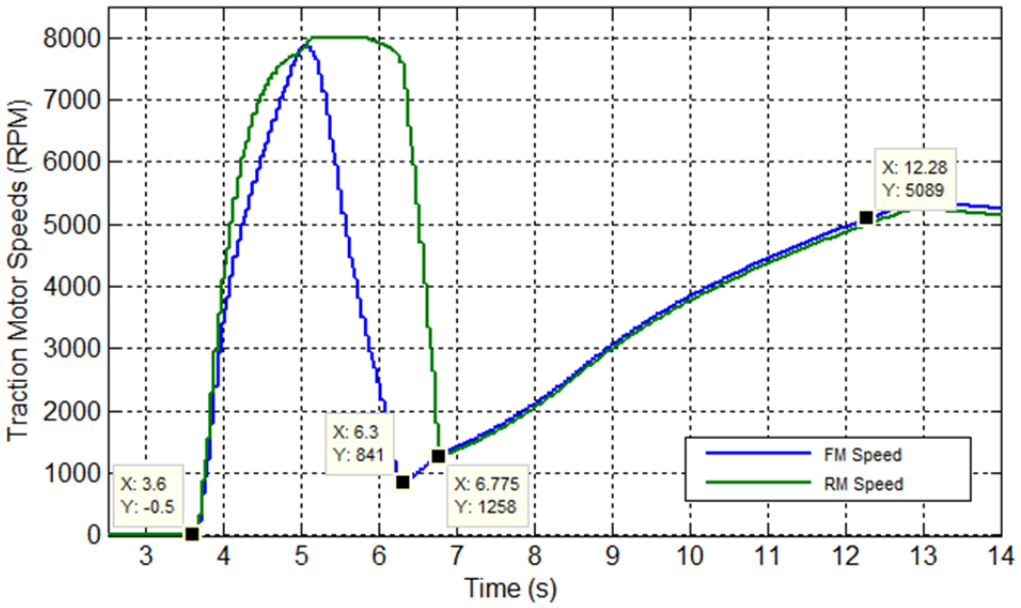

Figure 4.15 Front and rear motor speeds during reduced traction WOT HIL test, with R_r set to 5 ms.

The faster reduction in speed is a result of the TCS matching the driver torque request at a rate of 5 ms as opposed to the 10 ms rate in Fig. 4.12. Figure 4.14clearly illustrates the TCS in action, with a graph of allowed torque (the output of the TCS) split between the front and rear motors. Figure 4.13 shows that the front and rear motor both begin to slip at about 3.7 seconds into the test. The front motor torque request is quickly reduced by the TCS, and then torque is applied back as the front wheels transition to the full traction zone.

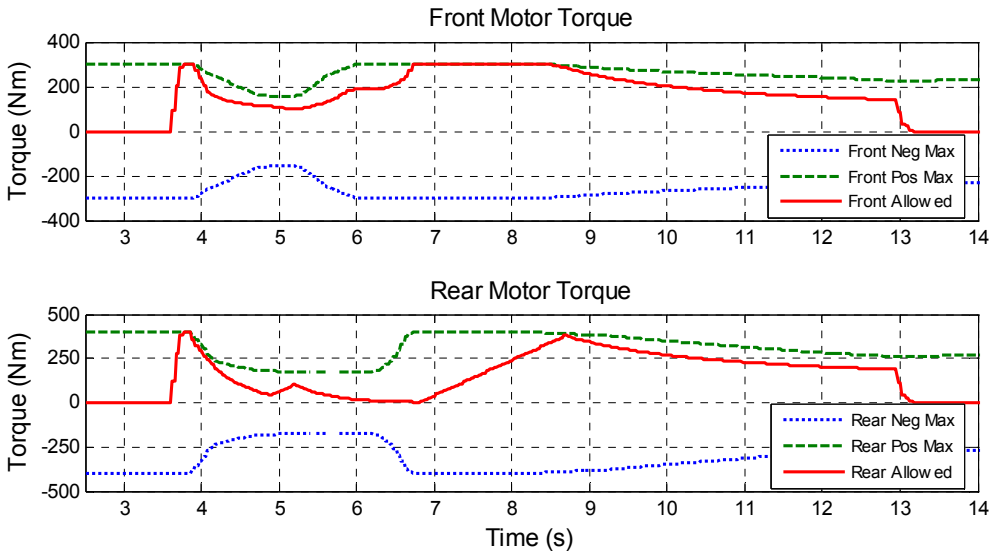

Figure 4.16 Output of the TCS during reduced traction WOT HIL test, with R_a set to 5 ms.

A closer look at the rear motor in Fig. 4.15 clearly defines when the TCS becomes active. The torque request is clearly reduced exponentially (see Eq. 8) when TCS has detected rear motor slip, and is linearly added back when the TCS is no longer detecting slip.

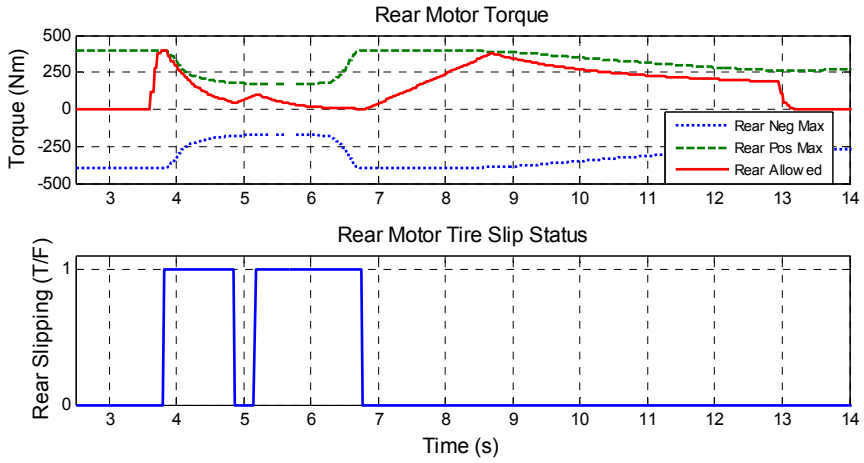

Figure 4.17 Comparison between rear motor torque request and slip detection for the rear wheels with R_r = 5 ms.

The R_r parameter was adjusted to 1 ms in the hopes that wheel slippage could be reduced even faster than with the 5 ms adjustment rate. Figure 4.16 shows the HIL simulation results of a reduced traction WOT test with R_r set to 1 ms.

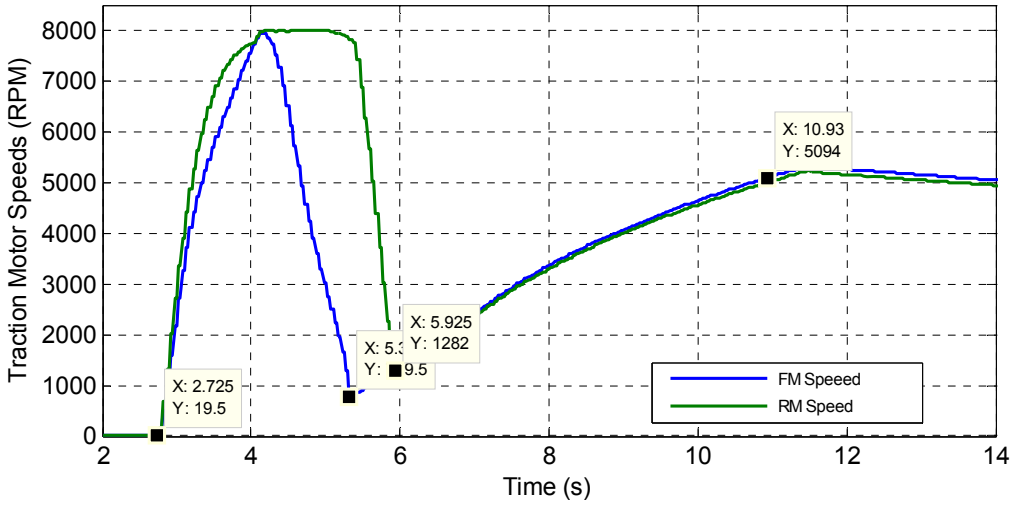

Figure 4.18 Front and rear motor speeds during reduced traction WOT HIL test, with R_r set to 1 ms.

As with the previous WOT test, Fig. 4.17 clearly shows the torque requests during the reduced traction WOT test, split up by front and rear motors. This time however, the matching slope is significantly higher due to the increased match rate, R_r.

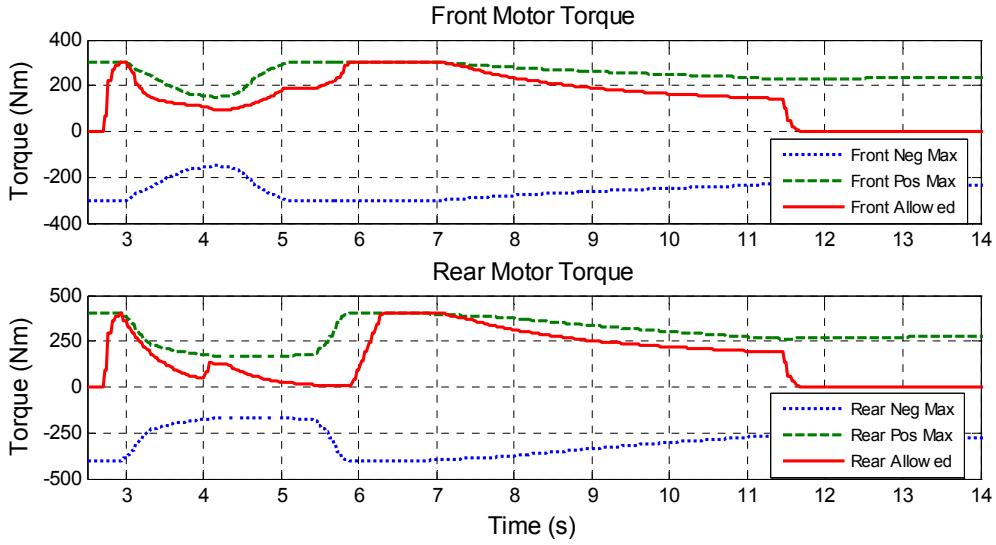

Figure 4.19 Output of the TCS during reduced traction WOT HIL test with R_a set to 1 ms.

A closer look at the rear motor torque request clearly defines when the TCS becomes active. An interesting note is that changing the match rate does not necessarily have the biggest effect on the time response of the TCS. A comparison between Fig. 4.17 and Fig. 4.14 shows that although the slope of the matching torque increases, it is the adjust scalar (S_a) parameter that could have the largest effect on response time. Although the S_a parameter could be tuned to the specific driveline, it was left unchanged for functional testing due to the impact that the parameter can have on driveline vibrations due to the mounting design of the powertrain components.

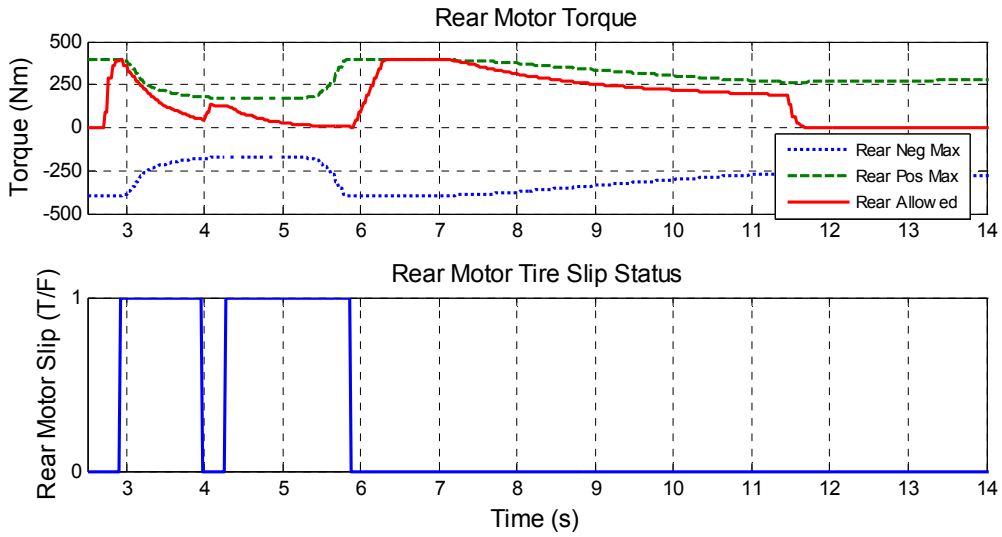

Figure 4.20 Comparison between rear motor torque request and slip detection for the rear wheels with R_r = 1 ms.

Table 4.5 summarizes the times recorded during the WOT testing for various values of R_r. Based on the data in the table, it can be concluded that the TCS is more effective at reducing the speed on the rear motor during this particular test. It is clear that the R_r of 10 ms did not appreciably change the time either of the motors was slipping, nor did it significantly affect 0-60 MPH (20 ms is negligible).

Table 4.5 Summary table of reduced traction WOT testing on HIL.

	Time (seconds)		
	FM Slip	RM Slip	0-60 MPH
No TC	2.53	4.08	8.23
R_r = 10 ms	2.55	4.13	8.25
R_r = 5 ms	2.70	3.18	8.68
R_r = 1 ms	2.63	3.23	8.23

The same experiments were repeated for in-vehicle validation testing, which was the last step of validation before the TCS could be fully implemented into the vehicle supervisory control system.

Overall, the TCS performed very similarly in all of the testing environments (HIL and in-vehicle). Differences between the tests are mainly due to the fact that the modeling for a reduced road surface frictional coefficient makes many assumptions that may not necessarily be true in the real world. In addition, the in-vehicle testing was done on gravel, which has a higher frictional coefficient than a wet road. Further discussion about the limitations of reduced traction modeling is discussed in Chapter V. The test results did, however, provide enough data to validate the functionality of the TCS under WOT conditions.

CHAPTER V

CONCLUSIONS

The project resulted in the successful design, simulation, and validation of three critical control systems for an all-wheel drive extended-range hybrid electric vehicle: power control, torque splitting, and traction control. The following objectives were met:

- Follow the industry standard development practice of SIL to HIL to In-Vehicle tests for controls development
- Ensure that each of the control systems operate independently of one another for robustness
- Improve vehicle handling in reduced traction environments by detecting wheel slip and modifying torque accordingly
- Improve efficiency and performance of the AWD electric drivetrain by developing a passive control strategy that maximizes the unique ability to split torque between front and rear motors
- Maximize the amount of energy that can be used and generated by the front and rear BLDC electric motors while staying within the limits of the ESS

Each system was tested in worst case driving scenarios (WOT and hard braking), and much was learned throughout the process, including areas for improvement.

The original component plant models were modified to match the vehicle once it was built in order to more closely simulate actual vehicle performance. The supervisory

controls development process then followed the intended development process of "in-the-loop" testing before "in-vehicle" testing, which was not possible without accurate simulation of the components used in the vehicle.

It was mandatory to develop the control systems presented in this thesis in the virtual world, given the nature of the control systems and when they are intended to be active (under high power, when the vehicle has lost traction, and splitting torque between front and rear motors). Simulation allowed for the simultaneous development of the three separate control algorithms without the need for a functioning vehicle, which reduced risk during the development process, and saved time and resources.

Areas for Improvement

Although the project was successful in developing three fully functional hybrid vehicle control systems, several areas for improvement were identified during the development process. These areas include:

- Develop a more complete plant model for the ESS
- Improve the tire slip model to include lateral forces
- Test the TCS in a dynamic event, such as auto-cross, or maximum lateral acceleration
- Tune the S_a and S_r parameters in the TCS to increase response time while maintaining consumer acceptability
- Validate torque splitting strategy with in-vehicle test data

Final Conclusions

The control systems that were developed improved vehicle performance in three distinct ways. The power control system improved the performance of the vehicle

drivetrain by maximizing the amount of energy that can be delivered to the wheels without overloading the energy storage system. The torque splitting strategy switched the vehicle from a mostly front-wheel drive efficiency mode into an all-wheel drive performance mode when aggressive driving behavior was detected, which improved straight line acceleration times. Lastly, the traction control system improved vehicle control by detecting and mitigating wheel slip during a loss of traction.

During the course of this project, three vital control systems were successfully designed, tested, and implemented into a hybrid supervisory control strategy for an all-wheel-drive extended range electric vehicle. The use of these systems seamlessly blends the vehicle controls with the driver while keeping the driver focused on the road and the controls focused on providing fully functional, yet safe, operation of the vehicle.

REFERENCES

[1] M. Ehsani, et al., “Modern Electric, Hybrid Electric, and Fuel Cell Vehicles: Fundamentals, Theory, and Design”. New York, CRC Press LLC, 2005, pp. 24-35,109-122, 239-257.

[2] R. Copparapu, D.S. Zinger, A. Bose, "Energy Storage Analysis of a Fuel Cell Hybrid Vehicle with Constant Force Acceleration Profile", *38th North American Power Symposium, 2006.,* pp.43-47, Sept. 2006.

[3] L. Wang, E.G. Collins, L. Hui, "Optimal Design and Real-Time Control for Energy Management in Electric Vehicles", *Proceedings of the 2011 IEEE Transactions on Vehicular Technology*, vol.60, no.4, pp.1419-1429, May 2011.

[4] J. Zhang, C. Yin, "Use of Fuzzy Controller for Hybrid Traction Control System in Hybrid Electric Vehicles", *Proceedings of the 2006 IEEE International Conference on Mechatronics and Automation (ICMA)*, vol. 3, pp.1351-1356, June 2006.

[5] R. Auffhammer, R. Heyken, H. Roth, “New Driving Stability Control System with Reduced Technical Effort for Compact and Medium Class Passenger Cars”, *Electronic Braking, Traction, and Stability Control, Automotive Electronics Series,* Society of Automotive Engineers, Inc., pp. 365-372, 1999.

[6] C. de Wit, P. Tsiotras, "Dynamic tire friction models for vehicle traction control", *Proceedings of the 38th IEEE Conference on Decision and Control*, vol.4, pp.3746-3751, 1999.

[7] Y. Hori, Y. Toyoda, Y. Tsuruoka, "Traction control of electric vehicle: basic experimental results using the test EV”, *IEEE Transactions on Industry Applications* , vol.34, no.5, pp.1131-1138, Sep/Oct 1998.

[8] M. Sojoodi, et al. "An Optimal Pole-Matching Observer Design For Estimating Tyre-Road Friction Force", Vehicle System Dynamics 48.10 (2010): 1155-1166. Academic Search Premier. Web. 28 Dec. 2011.

[9] J. Kang, J. Yoo, K. Yi, "Driving Control Algorithm for Maneuverability, Lateral Stability, and Rollover Prevention of 4WD Electric Vehicles With Independently Driven Front and Rear Wheels", *IEEE Transactions on Vehicular Technology*, vol.60, no.7, pp.2987-3001, Sept. 2011.

[10] B. Boning, R. Folke, K. Franzke, "Traction Control (ASR) Using Fuel-Injection Suppression – A Cost Effective Method of Engine-Torque Control", *Electronic Braking, Traction, and Stability Control, Automotive Electronics Series,* Society of Automotive Engineers, Inc., pp. 287-294, 1999.

[11] D. Yin; S. Oh; Y. Hori, "A Novel Traction Control for EV Based on Maximum Transmissible Torque Estimation", *IEEE Transactions on Industrial Electronics*, vol.56, no.6, pp.2086-2094, June 2009.

[12] L. Chenglin, L. Shoubo, C. Shanglou, W. Lifang, "Modeling and simulation of traction control of Hybrid Electric Vehicle", *International Conference on Mechatronics and Automation (ICMA), 2009*, pp.3252-3256, Aug. 2009.

[13] R. Vijayagopal, A. Rousseau, "System Analysis of Multiple Expert Tools", SAE 2011-01-0754, SAE World Congress, Detroit, April 2011.

[14] M. Teraoka, "Development of the Electro-Magnetic Controlled Limited Slip Differential Unit", *Electronic Braking, Traction, and Stability Control, Automotive Electronics Series,* Society of Automotive Engineers, Inc., pp. 309-317, 1999.

APPENDIX A

DESCRIPTIONS OF VALIDATION TESTING

Wide Open Throttle (WOT) Test

WOT testing is simulated by linearly ramping the throttle from zero to 100% in 0.25 s. The accelerator is decreased back to zero in the same fashion once the vehicle has reached 60 mph. The vehicle then coasts to 50 mph before the accelerator is again ramped back to 100%. The accelerator pedal is decreased again to zero and the test is finished once the vehicle reaches 70 mph. This test is intended to validate off-the-line acceleration as well as highway passing acceleration.

A modified WOT test was performed to validate the traction control portion of the drivetrain controller. For this test, the vehicle begins WOT on a reduced traction patch of road. The vehicle is required to drive out of the reduced traction segment and onto a dry road surface with WOT applied. Due to the emphasis of the transition between reduced and full traction, only the first portion (0-60 mph) of the test was performed.

Braking Test

The braking test is performed by accelerating the vehicle to 70 mph and applying a pre-determined, constant, amount of brake pedal travel until the vehicle reaches a desired speed. For the purpose of validating power control, this test was run once with 10% brake pedal travel and again with 50% brake pedal travel.

Reduced Traction Testing

The traction control portion of the vehicle control strategy was tested throughout all three stages of development. Slip detection was validated in the offline simulation environment through the application of simple test cases to force the state machine through all of the states in the traction control algorithm. A unique method for modeling a loss of traction was developed which allowed a fully functional traction control system

to be developed and validated in a purely virtual environment before in-vehicle testing began.

A WOT test was performed under full traction, as well as reduced traction road conditions. For HIL testing, the road frictional coefficient, μ, was varied between 0.2 (low traction) and 1 (full traction) as the vehicle moved forward on the test surface. For in-vehicle testing, the vehicle began the test in a gravel road, and transitioned to dry pavement. Figures A.1-A.3 give a graphical representation of how the reduced traction WOT tests were performed both in the HIL and in-vehicle environments.

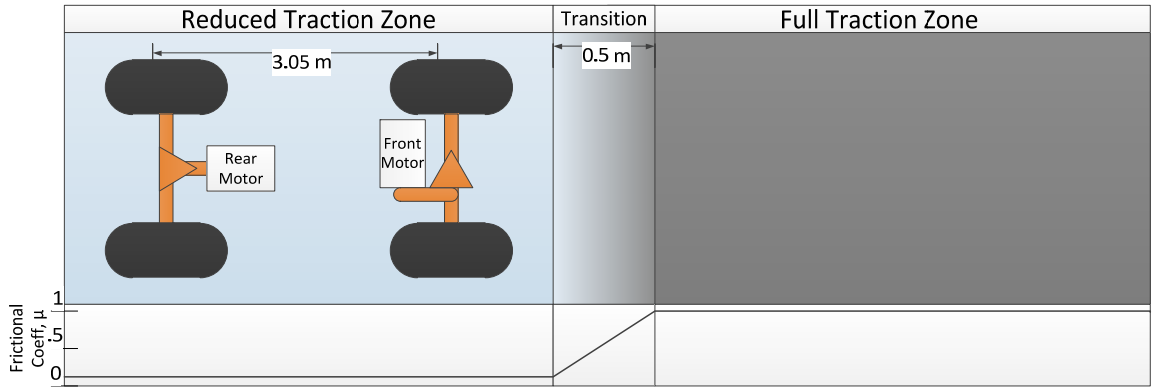

Figure A.1 Vehicle begins WOT test in reduce traction environment.

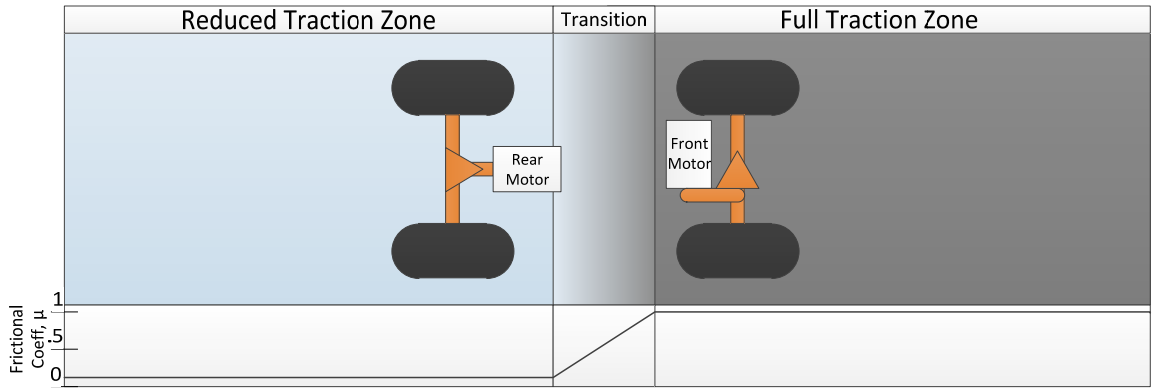

Figure A.2 WOT is applied, and as the vehicle moves forward, the front wheels transition to full traction first.

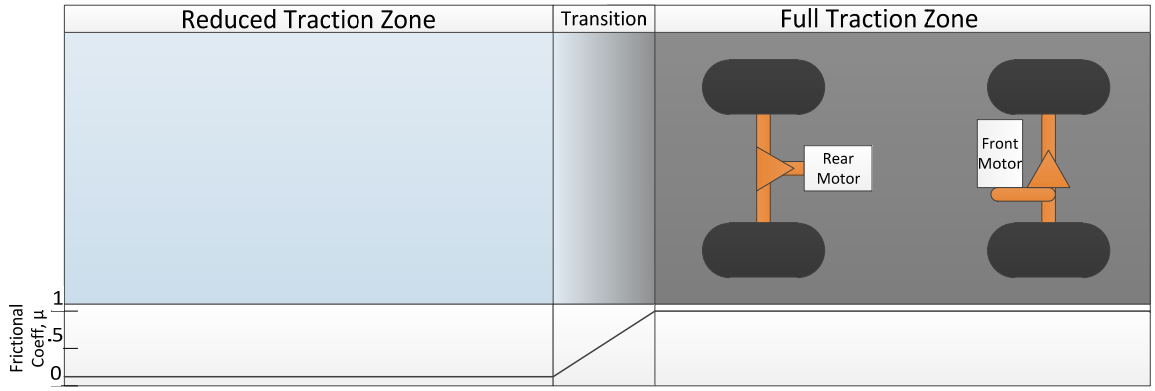

Figure A.3 The rear wheels complete the transition to the full traction zone as the vehicle leaves the reduced traction zone.

This method of testing the traction control system verifies that the traction control algorithms successfully manage the torque requests for each of the motors independently, based on design of the traction control system.

APPENDIX B

SLIP DETECTION DIAGRAM

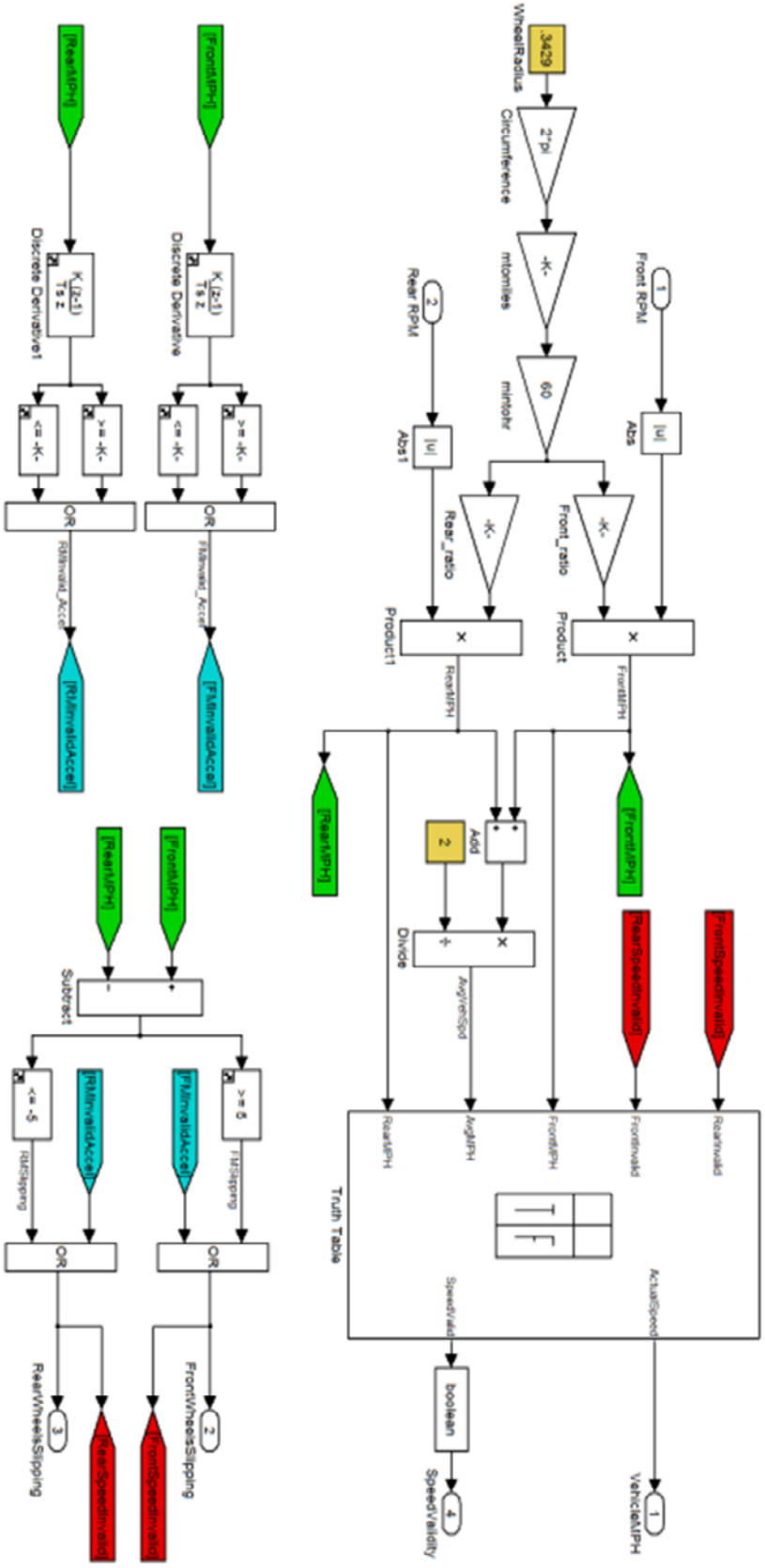
WheelRadius
3429
Circumference
2*pi
mtomiles
mintohr
60
Front RPM
Rear RPM
Abs
Abs1
Rear_ratio
Front_ratio
Product1
Product
RearMPH
FrontMPH
[RearMPH]
[FrontMPH]
Add
2
Divide
AvgMPH
[RearSpeedInvalid]
[FrontSpeedInvalid]
RearInvalid
FrontInvalid
RearMPH
AvgMPH
FrontMPH
Truth Table
T
F
SpeedValidity
ActualSpeed
boolean
SpeedValidity
VehicleMPH
[RearMPH]
[FrontMPH]
Discrete Derivative1
Discrete Derivative
K (z-1) Ts z
<= -K-
>= -K-
OR
RMInvalid_Accel
FMInvalid_Accel
[RMInvalidAccel]
[FMInvalidAccel]
[RearMPH]
[FrontMPH]
Subtract
<= -5
>= 5
RMSlipping
FMSlipping
OR
RearWheelsSlipping
FrontWheelsSlipping
[RearSpeedInvalid]
[FrontSpeedInvalid]

APPENDIX C

SIL SIMULATION AND VALIDATION TESTING RESULTS

Power Control Testing

Two tests were performed during SIL simulations to validate the power limiting strategy: WOT and Regenerative Braking. Figure C.1 illustrates the inputs to the system (brake pedal and accelerator pedal) and the simulation output (vehicle speed).

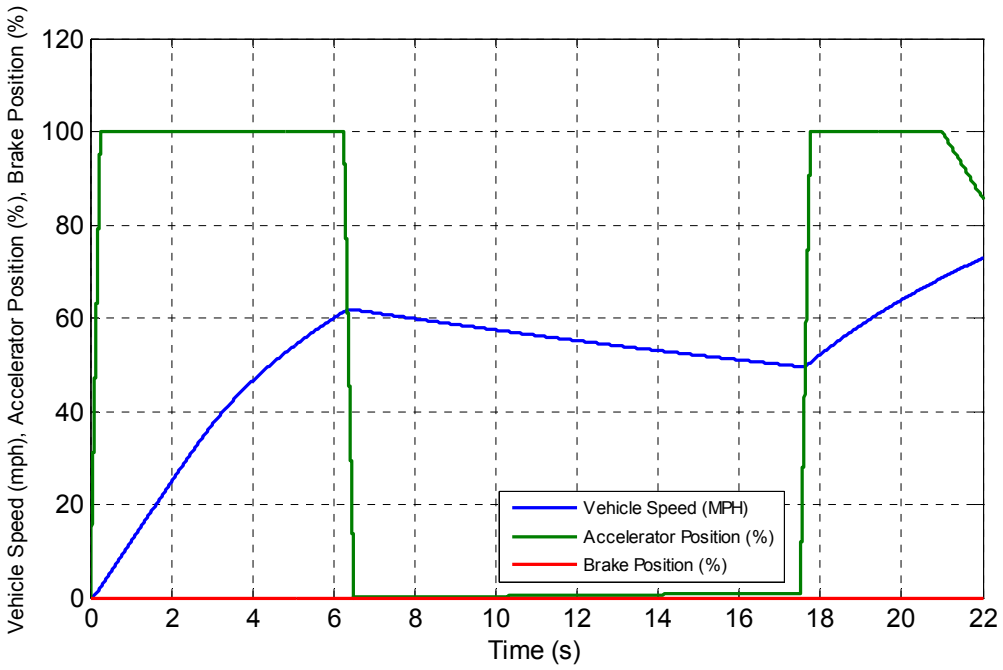

Figure C.1 SIL WOT test input and resulting vehicle speed.

The following figures contain additional data that was collected during the WOT test. Each graph shows the calculated available discharge and charge maximum power and torque limits superimposed on top of the actual power and torque used. The graphs clearly illustrate whether or not the power limiting strategy is effectively controlling the power usage of the system.

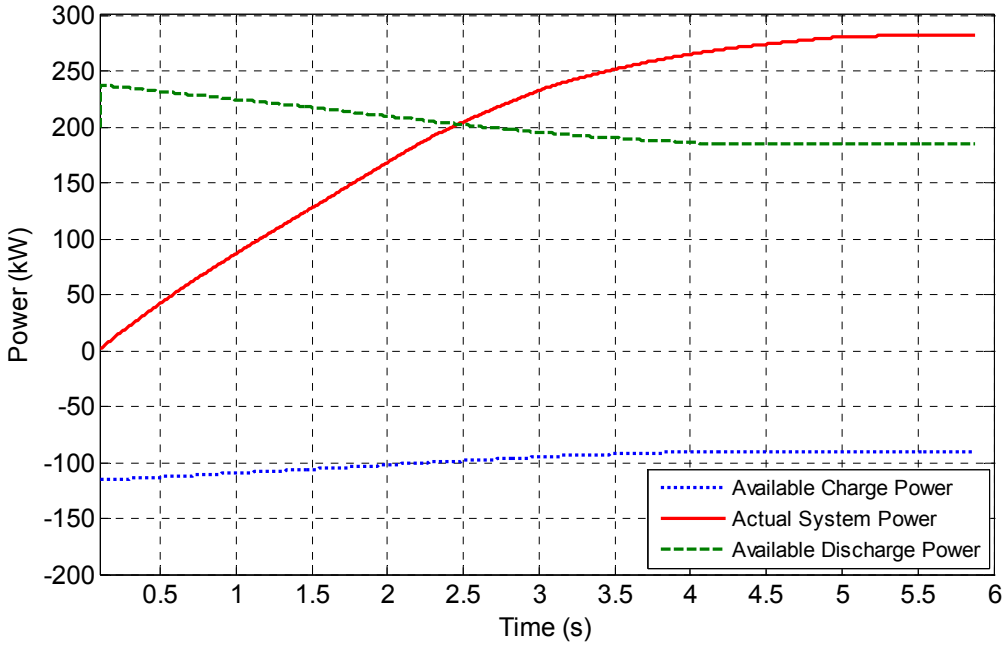

Figure C.2 Wide-Open Throttle (WOT) without power limiting or traction control.

Without active power limiting, the drive motors will attempt to draw more power than the battery controller will allow. Under full throttle conditions, the power draw exceeds the battery power capability by almost 100 kW as seen in Fig. C.2. Due to limitations imposed by the battery controller to maintain safe operation of the battery, this type of over-power situation is not possible on the actual vehicle. Without power limiting, the battery controller goes into an Emergency Power Off (EPO) state, and opens the contactors regardless of the current flowing through them. This action disables the high voltage bus, and in turn, the vehicle. In addition, opening the contactors under high power loads increases the possibility of welding the contacts closed and significantly reduces the operating life of the contactors due to the plasma arc that is drawn as the contacts open. The available discharge power decreases over time due to the voltage drop of the battery pack during maximum discharge conditions.

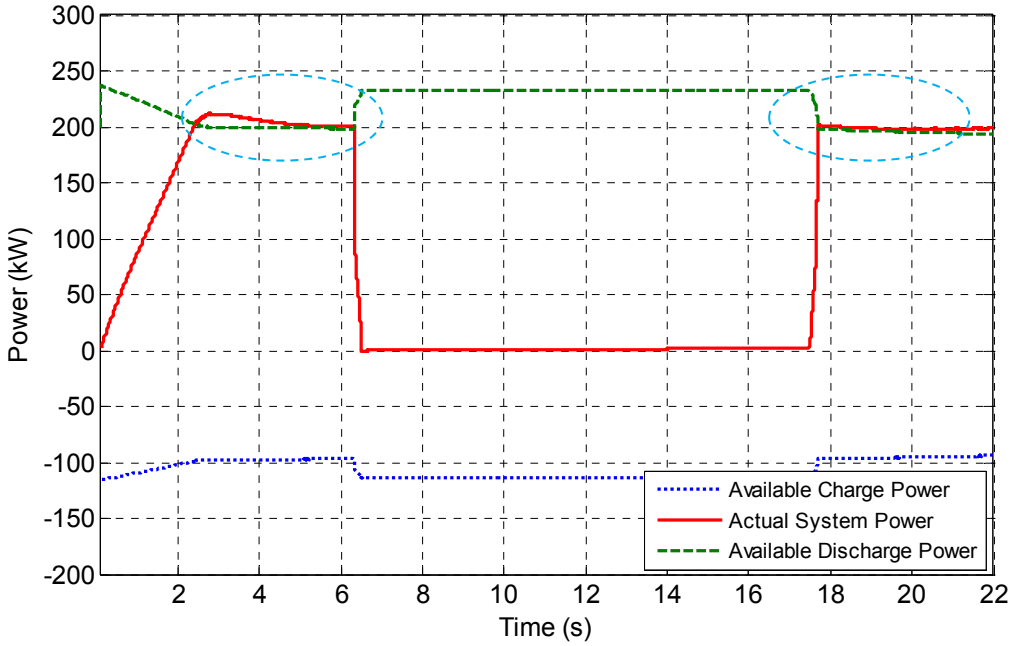

Figure C.3 Wide-Open Throttle (WOT) with power limiting active.

Figure C.3 shows that the system responds to the power limits of the power sources instead of the power limits of the drive motors. The circled region indicated the over-power regions of the strategy. The long period of near-zero power consumption is due to the vehicle coasting from 60 miles per hour to 50 miles per hour, as required by the test. As WOT is re-applied at 50 miles per hour, the power control strategy re-activates, but responds much more quickly once the limit has been exceeded.

Figure C.2 shows the initial 0-60 mph acceleration with the power control algorithm disabled, emphasizing the split between the front and rear motors.

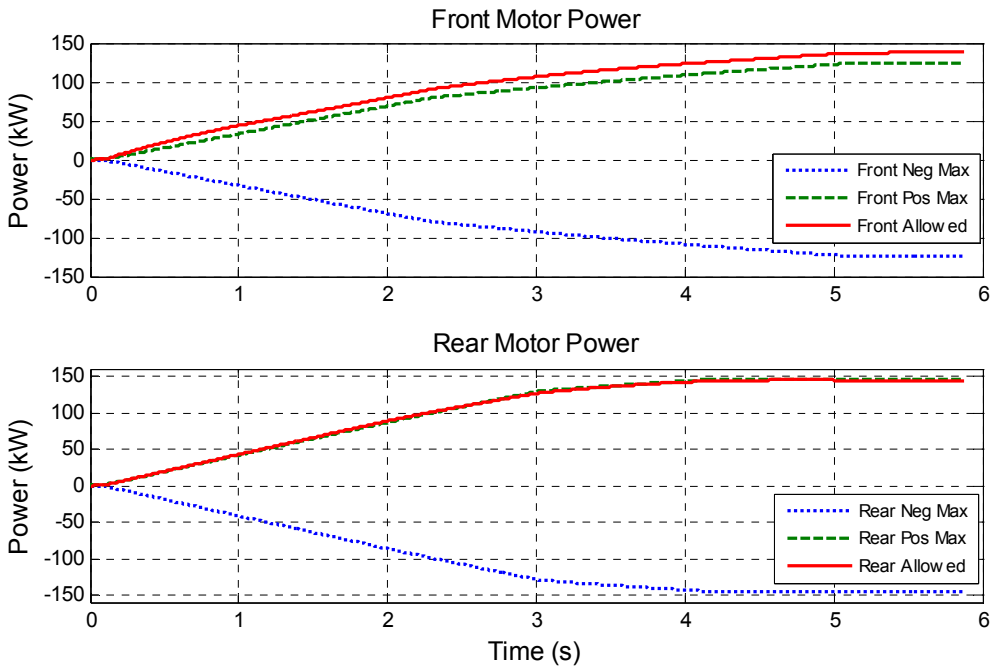

Figure C.4 Power comparison between motor limits and power usage of each of the drive motors without power limiting enabled during WOT.

Note that without power control, each motor follows the maximum power curve of the motor at all times. Figure C.5 shows the effect of the power limiting strategy related to each motor's power consumption. Note that as the actual power curve falls below the maximum power curve of each motor as the power control strategy follows the limits of the battery instead of the motors.

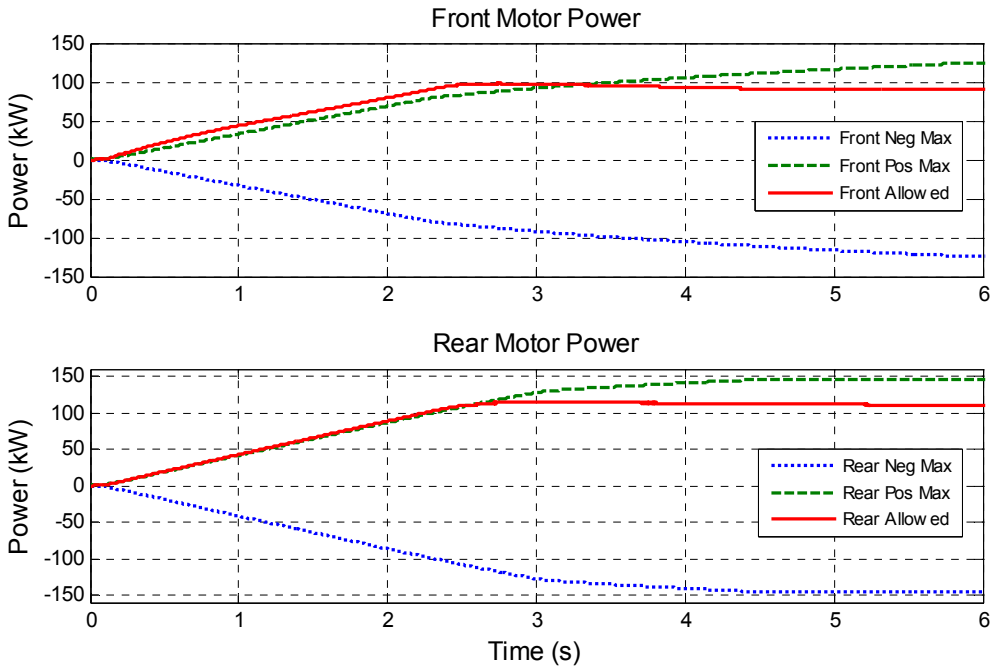

Figure C.5 Power comparison between motor limits and power usage of each of the drive motors with power limiting enabled during WOT.

The motors in the test vehicle are torque commanded, which means power usage is actually a result of a commanded torque at a given speed. Figure C.6 illustrates the commanded torque compared to the calculated available torque of each motor during a WOT test with power control deactivated.

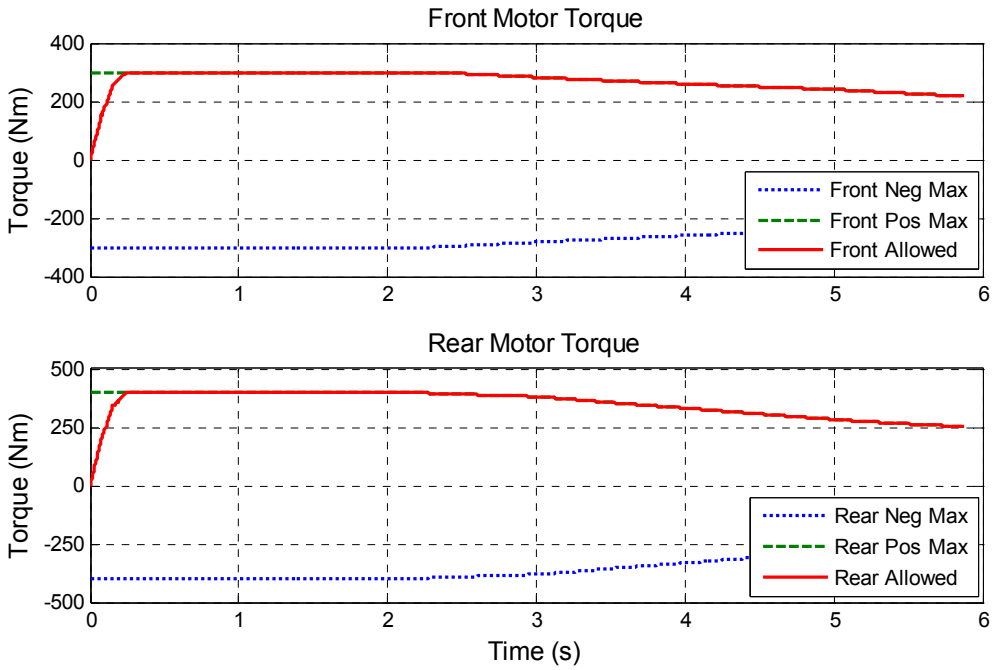

Figure C.6 Torque comparison between motor limits and torque requested with power limiting disabled during WOT.

One may note that without power control, the drive motors follow the maximum torque curve of the motor at all times. Figure C.7 shows that the requested torques fall below the motor maximum limits as the power control strategy follows the limits of the battery when the power control algorithm is activated.

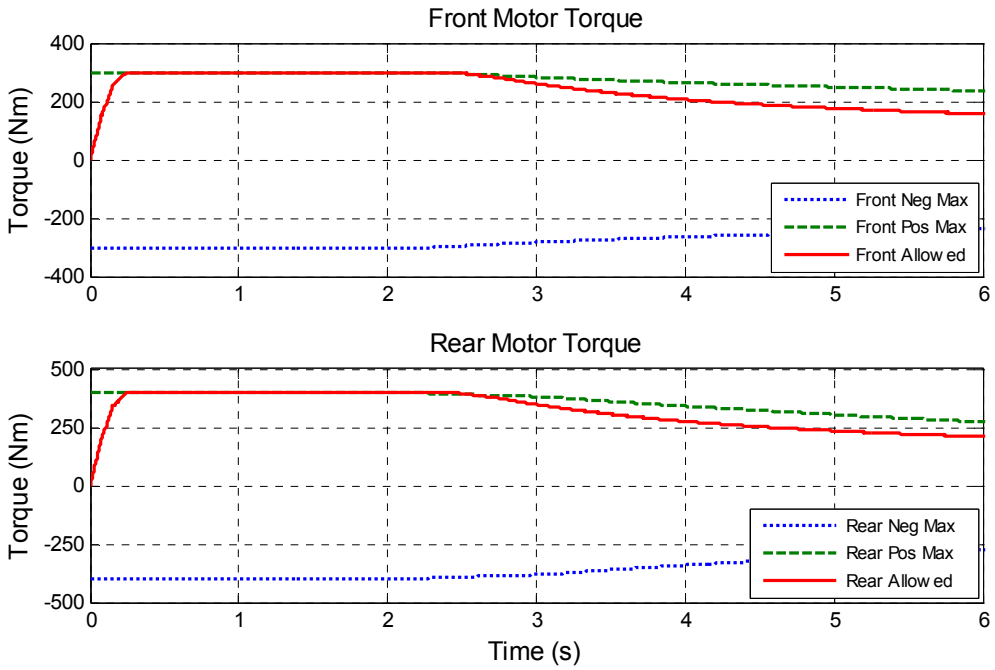

Figure C.7 Torque comparison between motor limits and torque requested with power limiting enabled during WOT.

The power control strategy must be capable of limiting the charging power in addition to the discharging power. As such, validation tests were developed to ensure the power control strategy performed flawlessly for both discharge and charging power conditions.

The following figures demonstrate the power control strategy test results for a constant brake pedal position at a beginning speed of 70 mph. Figure C.8 illustrates the vehicle speed and pedal positions during the regenerative braking test.

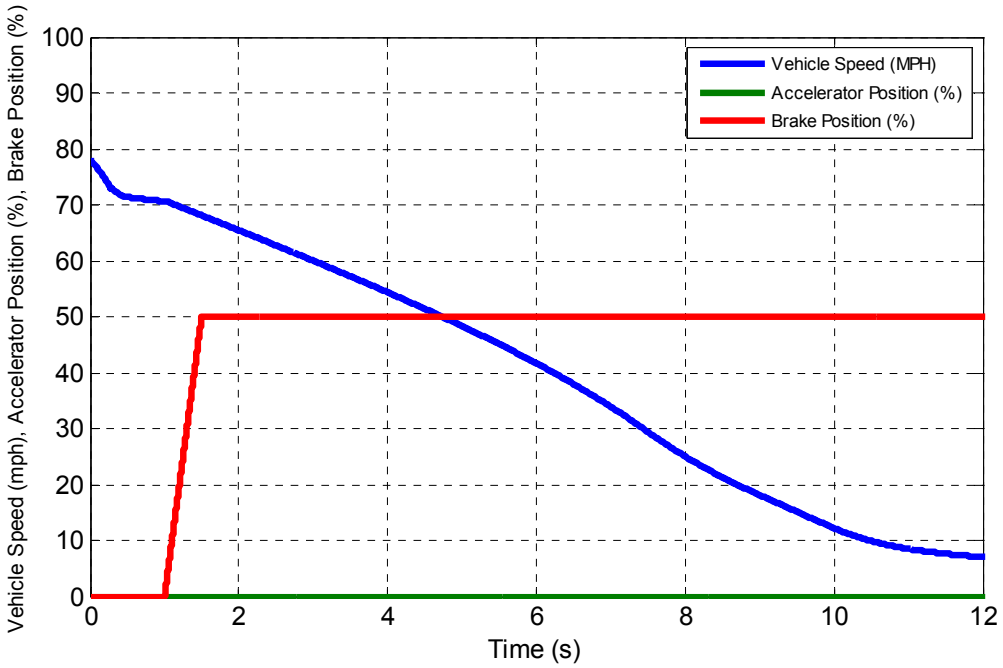

Figure C.8 Regenerative braking SIL test inputs and resulting vehicle speed.

The following graphs represent the power and torque data that was collected during the braking SIL test. Figure C.9 shows that the regenerative power remains at the limit of the battery during the entirety of the braking event until the regenerative brakes transition to mechanical brakes at low speed.

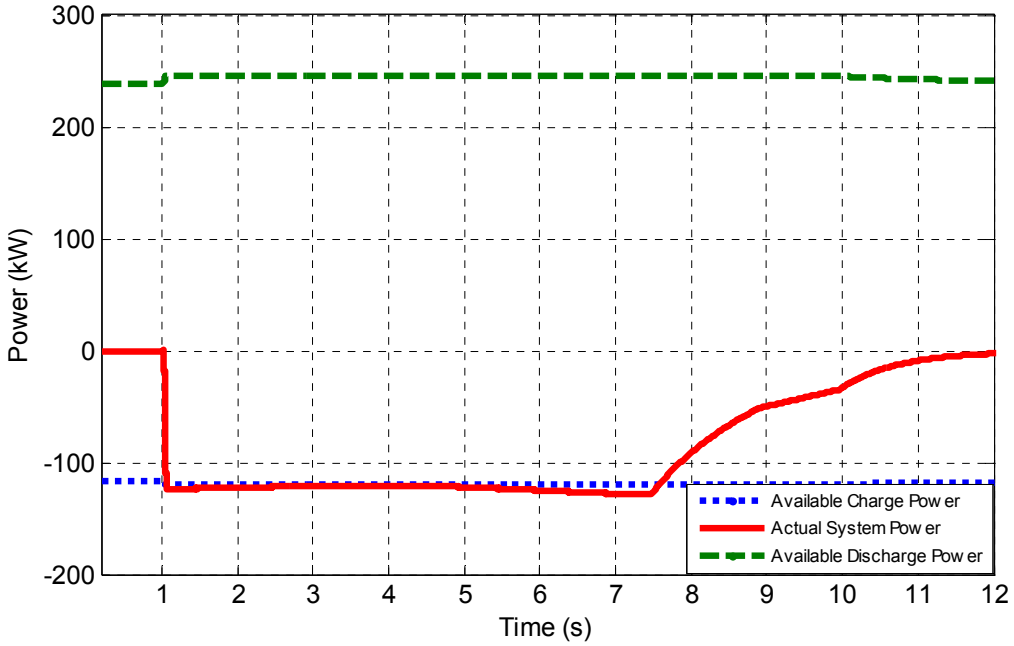

Figure C.9 Available and actual system power during regenerative braking.

Figure C.10 illustrates the calculated available torque compared to the actual torque request being sent to the motors. It is clear the torque command follows the limits of the battery's charging power.

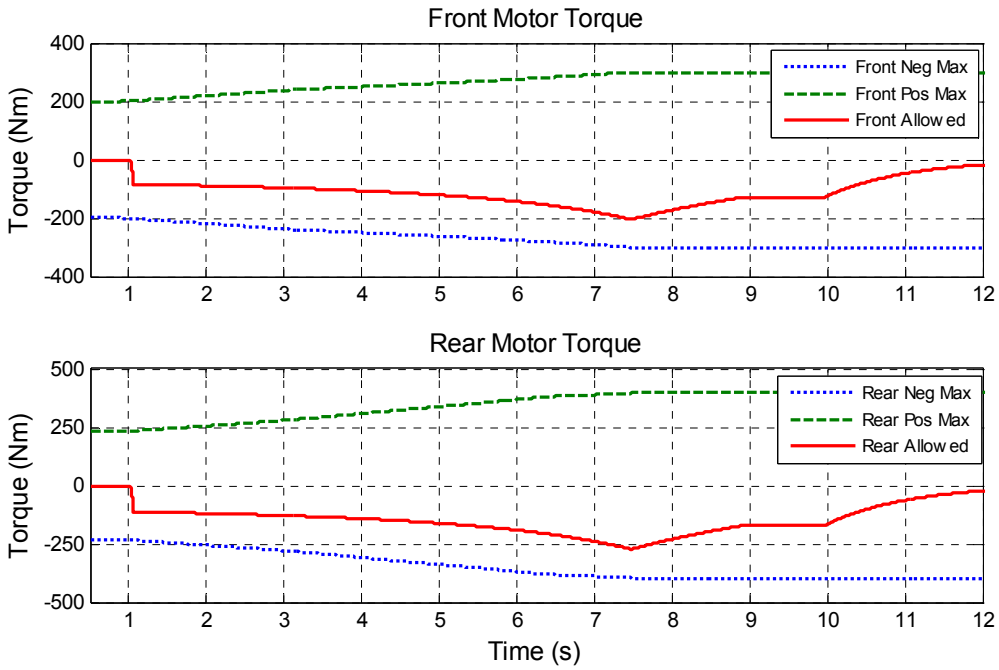

Figure C.10 Torque comparison between motor limits and torque requested with power control enabled during regenerative braking.

As Fig. C.10 shows, the actual torque curve follows a similar curve as the limits of the motor, except the actual torque is scaled to a value that stays within the power limits of the battery. Figure C.11 illustrates the power usage of both motors during the same test.

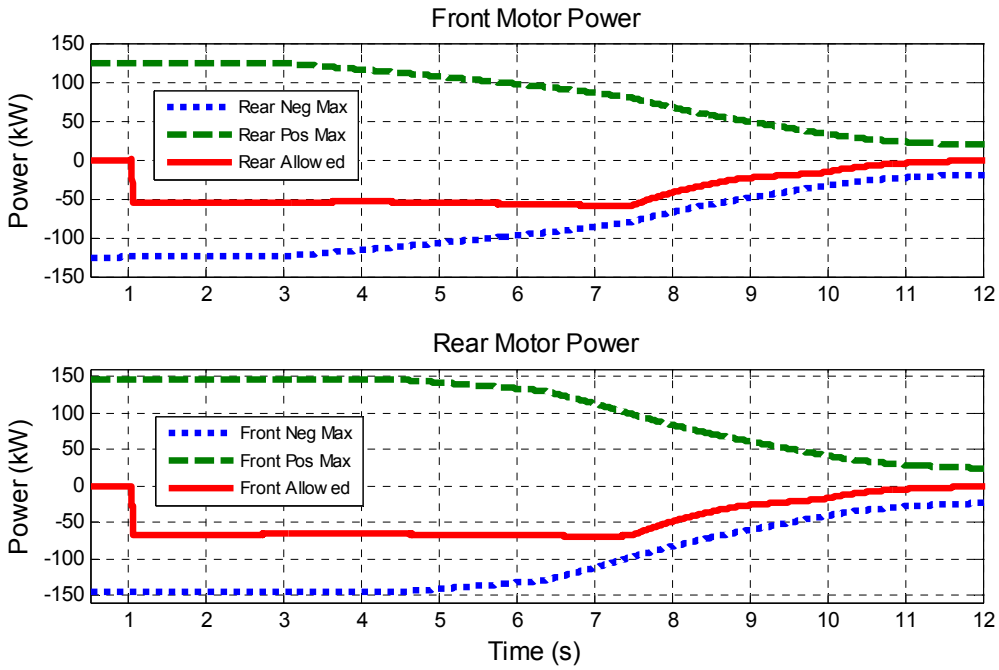

Figure C.11 Power comparison between motor limits and actual power used with power control active during regenerative braking.

Figures C.3 – C.11 illustrate that the power control strategy does, in fact, force the standard power and torque curves to be within the limits of the battery's capabilities. SIL simulation results prove that the power limiting strategy performs as designed. The next step of validation is to flash the new control algorithms onto the vehicle's supervisory controller in order to test the controller in real-time using a HIL simulator.

APPENDIX D

IN-VEHICLE TEST RESULTS

Power Control

In-vehicle validation testing of the power control strategy was the last step of the strategy development process. The same tests were performed as with SIL and HIL testing. The following figures show actual vehicle performance with power control enabled. Due to physical safety concerns, in-vehicle testing without power control enabled was not performed in order to minimize the risk of physical harm to the driver, as well as damage to components during testing. In addition, only the first portion of WOT testing was performed (0-60 mph acceleration) due to limited closed track testing space. Figure D.1 illustrates the pedal inputs and resulting vehicle speed during the in-vehicle WOT test.

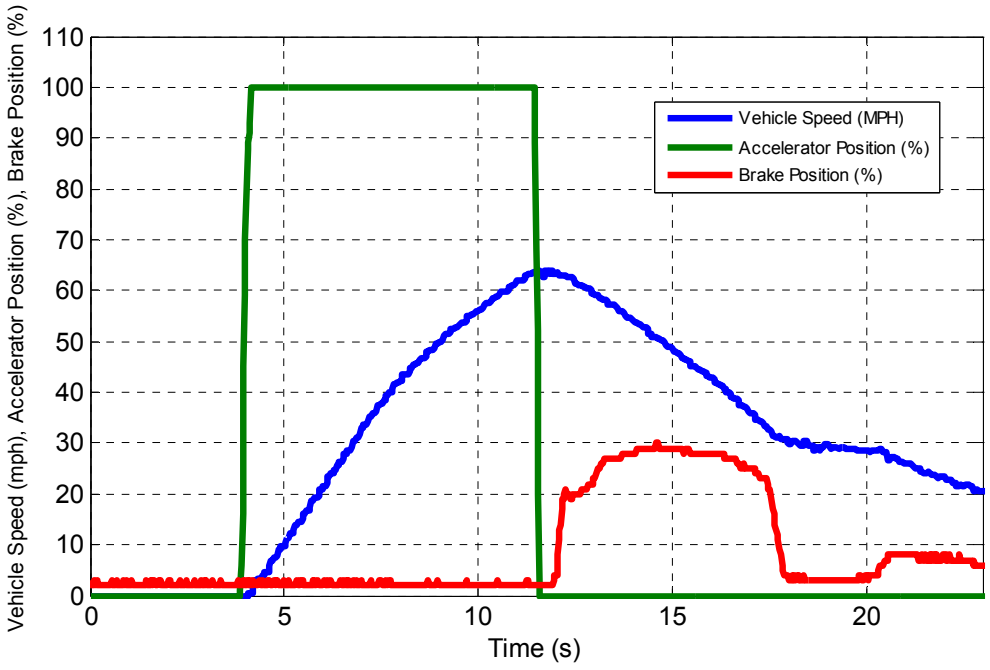

Figure D.1 Pedal inputs and resulting vehicle speed for in-vehicle WOT test.

Note that the brake was applied shortly after the vehicle reached 60mph. This is due to the limited track distance, which resulted in the need to decelerate the vehicle immediately after a vehicle speed of 60 mph was achieved. Figure D.2 shows the available system power and the actual system power.

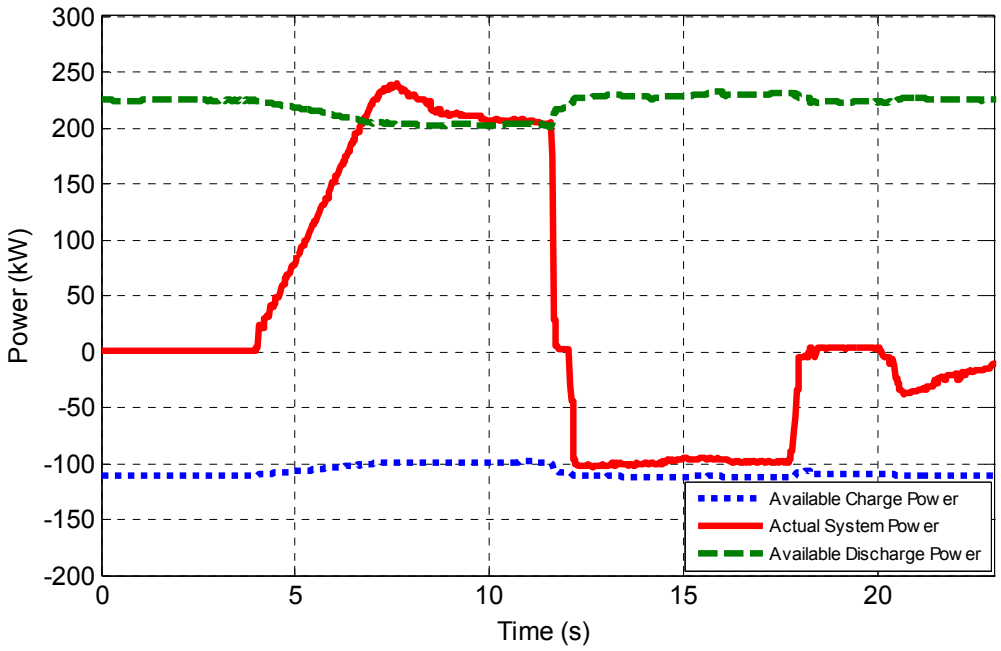

Figure D.2 Total available system power and actual power used and generated.

As with SIL and HIL testing, the power control algorithm allows the motors to overpower the battery for a short amount of time before limiting the discharge power back to the limit of the battery. The in-vehicle test was slightly different due to the limited track space, but this difference allowed the power control algorithm to highlight both discharge and charge power limiting in the same test. Almost immediately after the accelerator is released, the power becomes negative due to the brake being pressed. It is clear that the power control algorithm performs exceptionally under both discharge and

charge conditions, even if the driver goes from one extreme to the other such as depicted in Fig.D.2.

Figure D.3 gives a closer look at the torque that is commanded by the power control system during the same WOT event.

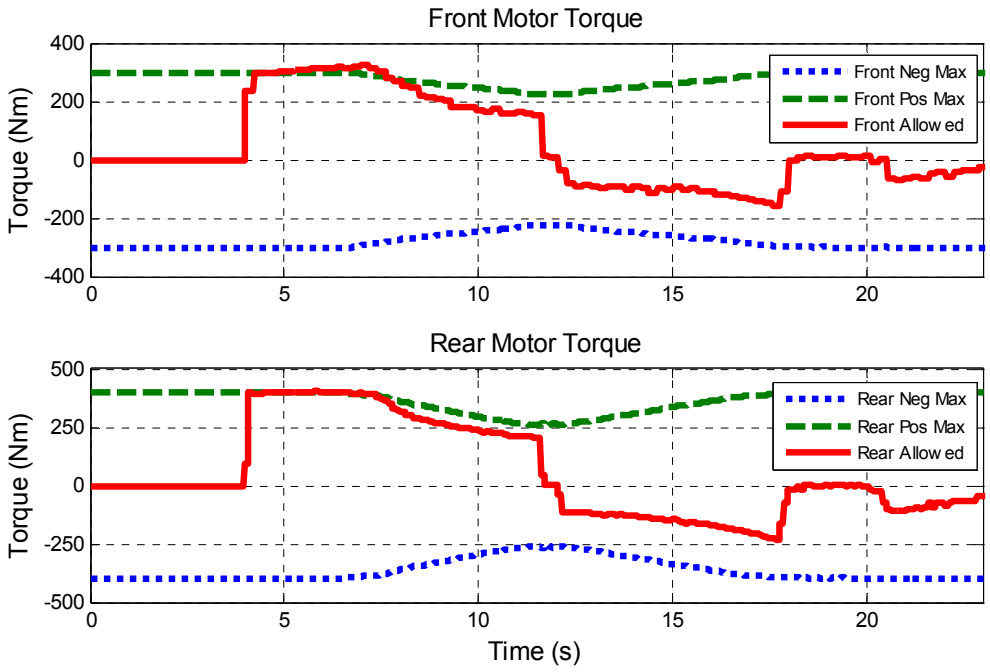

Figure D.3 Torque comparison between motor limits and torque requested with power control enabled during WOT.

It is clear that the power control system allows full torque on both motors for a short period of time before limiting the torque request to match the power capabilities of the battery. The trace appearance of being "wobbly" is due to a Nyquest sampling issue between the data recorder and the data transmission rate of 20 ms from the motor controller. Since data was collected at a sample rate of 1 ms, the resulting trace is a stepped function in some places.

Figure D.4 provides a closer look at the resulting power consumption and generation from each of the drive motors during the in-vehicle WOT test. The limited power traces (red) clearly follow the maximum discharge and charge power limits until the system power reaches the limit of the battery. Once the limit is reached, the system adjusts torque command, which in turn reduces the power that is consumed by each of the motors.

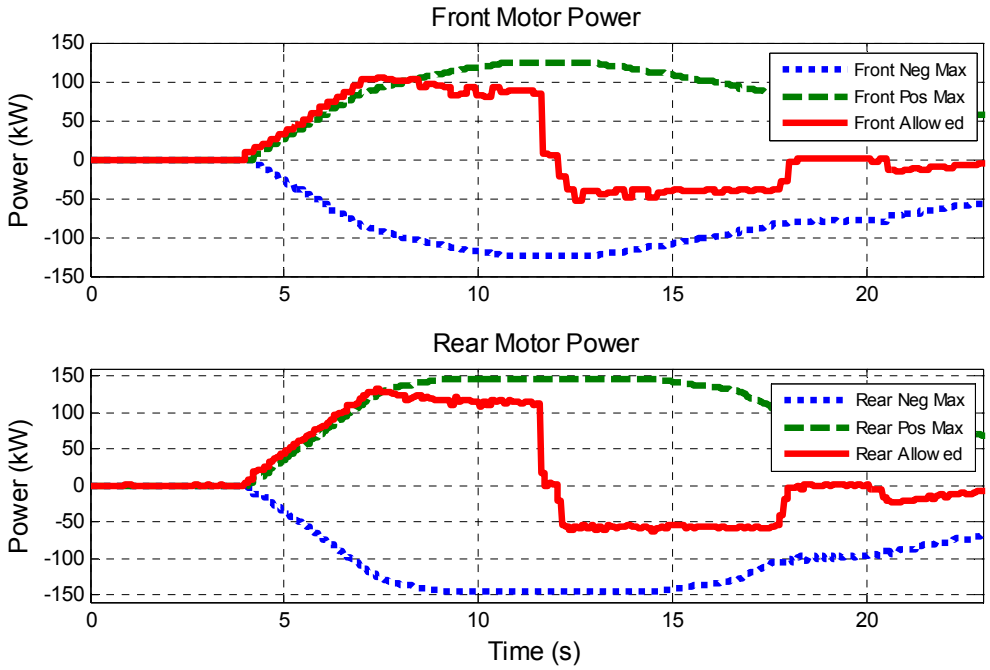

Figure D.4 Power comparison between motor limits and actual power used with power control active during WOT.

The in-vehicle testing results match the simulated testing results from both SIL and HIL almost exactly.

Traction Control

Figure D.5 illustrates the mitigation process in an in-vehicle WOT test, starting out on a gravel surface and transitioning to a smooth paved surface.

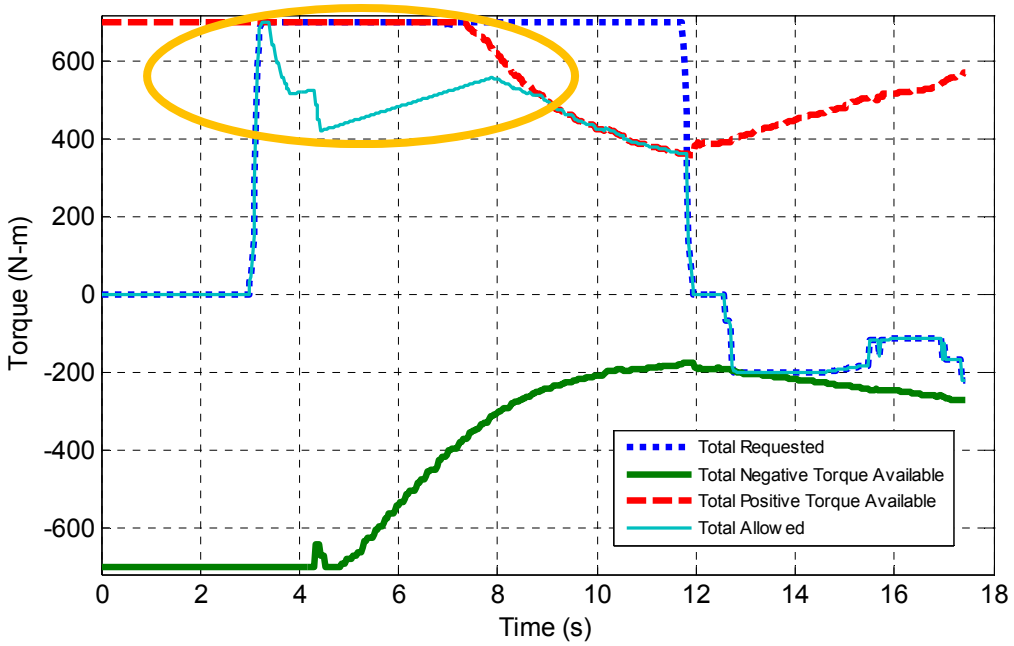

Figure D.5 The different stages of the torque calculation portion of the vehicle controller, identifying the active TCS.

The motor speeds are constantly monitored, ensuring that the system will detect slip even when torque is being reapplied. This can be seen in Fig.D.5 as the short step within the circled portion of the graph. The system automatically exits the active torque reduction when certain conditions are met. The traction control system also contains an indicator flag, letting the rest of the control strategy (and the driver) know when the traction control system is active. Due to the design of the torque calculation portion of the vehicle controls, the traction control system is the final stage of torque manipulation before the command is sent to the motor controllers. As a result, this stage can alter the torque regardless of which operational mode the vehicle is in (Charge Sustain, Charge Deplete, Limp Home). This feature ensures that the vehicle's torque command will always be first and foremost committed to ensuring that the wheels stay connected to the road. In-vehicle testing of the reduced traction WOT test was done with R_r fixed to 1 ms.

All four wheels were placed on a gravel road, and WOT was applied. The vehicle then transitioned from a gravel road to a pavement road after traveling roughly 3 m. This test is exactly the same format as the HIL test, so the same reduced traction testing procedure was used. Figures D.6-D.10 show the in-vehicle test results of the TCS with the R_r variable fixed to 1 ms.

Similar to the HIL testing, Fig.D.6 serves as the control for in-vehicle validation testing by showing the results of the reduced traction WOT test with TCS disabled. An interesting note is that the rear motor did not slip on the gravel surface as would be expected, even with the TCS disabled. The step-like waveforms are due to the front and rear motor controller sending the status message (containing the motor RPM) every 200 ms.

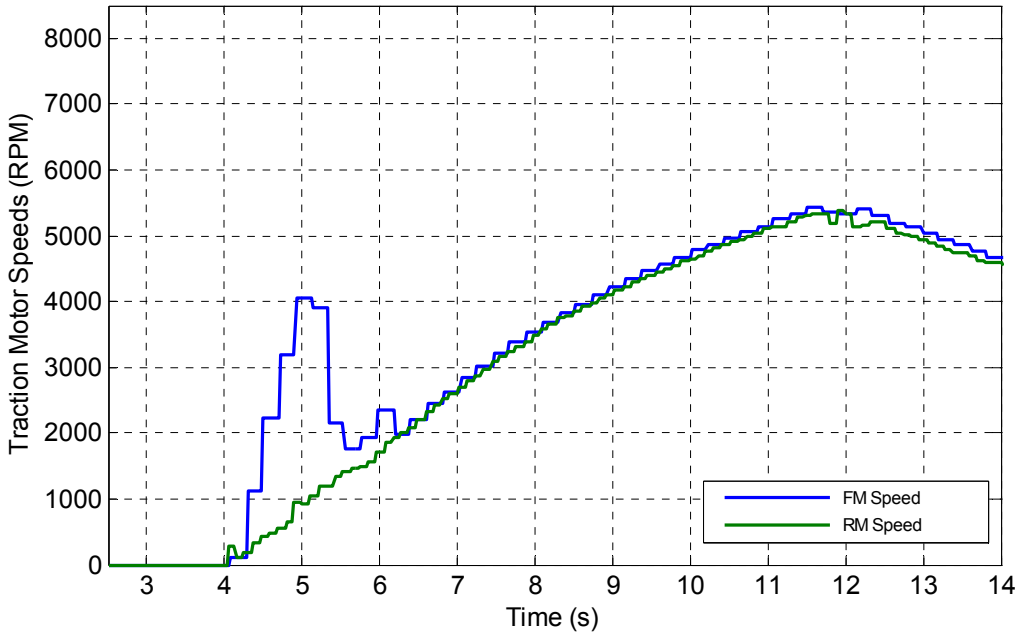

Figure D.6 Front and rear motor speeds for in-vehicle WOT test with reduced traction and no traction control.

Figure D.7 shows the same WOT test with TCS enabled. It is interesting to note that the TCS detects wheel slip much faster than in the HIL simulations, which results in much lower RPM "bumps".

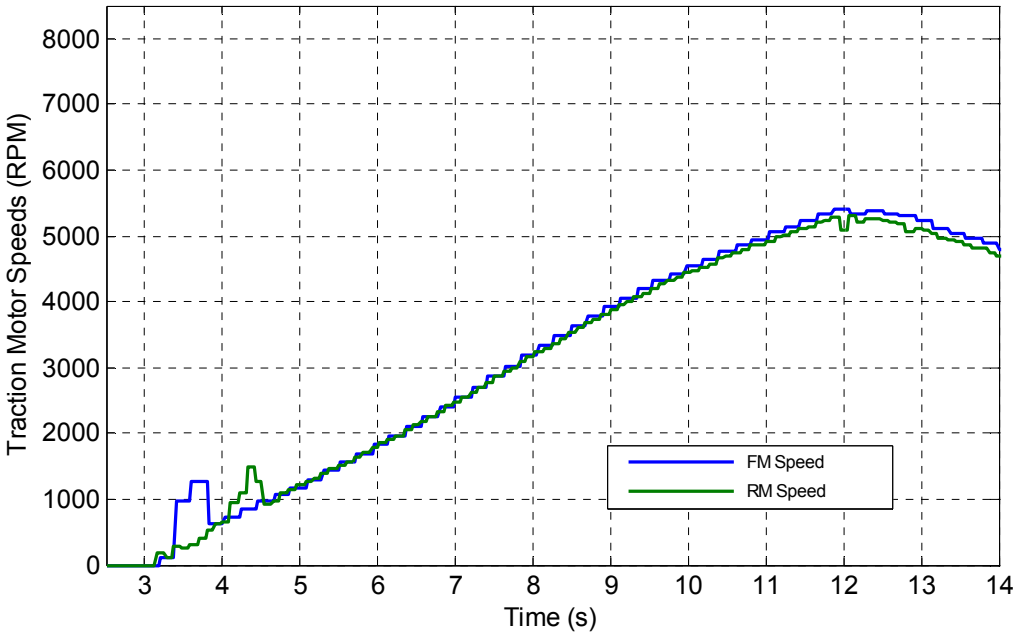

Figure D.7 Front and rear motor speeds for in-vehicle reduced traction WOT test, with R_r = 1 ms.

A more complete picture of the downstream torque (including graphs of requested, available, and allowed torque) is presented in Fig. D.8. This graph is useful for determining where the allowed torque deviates from the requested torque. If the allowed torque follows the curves of the maximum negative or positive available torque, it can be deduced that the TCS is not overriding the driver input. Likewise, when the allowed torque deviates from both the requested torque and the available torque lines, it can be deduced that the TCS is overriding the driver input and forcing the allowed torque to follow the designed algorithm.

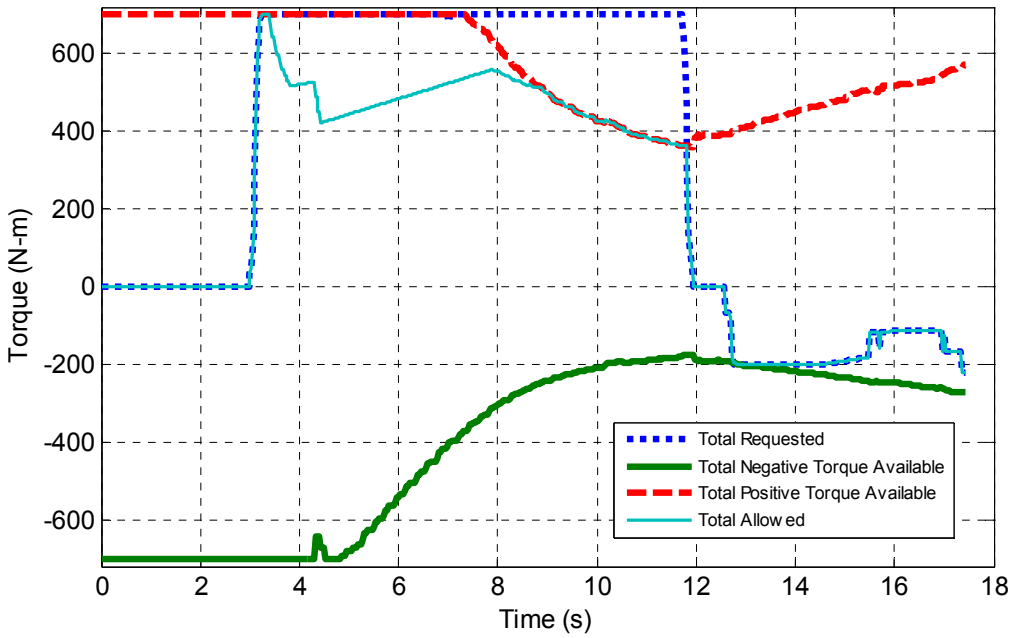

Figure D.8 Downstream torque limiting showing initial driver input (torque request) all the way to the output of the TCS (allowed torque).

Figure D.9 shows the allowed torque request that is sent to each motor. The amount of torque that is sent to each motor is determined by the "Torque Split" algorithm, which is described in Chapter II. In this case, as well as all of the TCS testing cases, the torque was split to act as a "Performance" mode, which meant that the torque was evenly split between the two motors as a percentage of their maximum available torque.

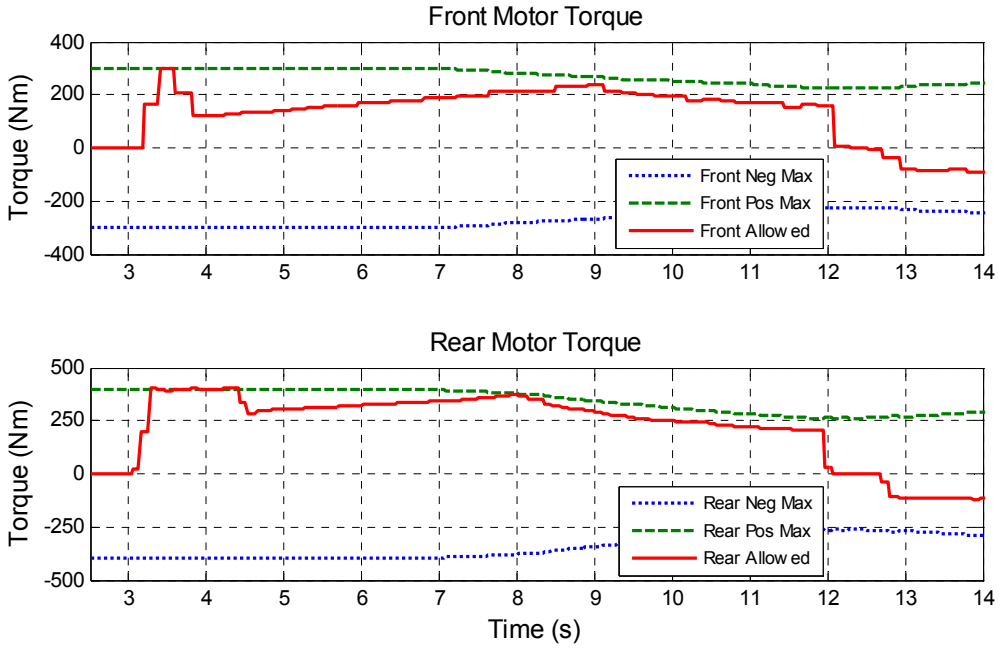

Figure D.9 Output of the TCS during an in-vehicle reduced traction WOT test, with R_r = 1 ms.

As with the HIL testing, a closer look into the individual motor torque requests reveals exactly when and how long the TCS was activated. The in-vehicle testing resulted in activating both the front and rear TCS at separate times. As a result, the front and rear torque requests are shown in Figs D.10 and D.11.

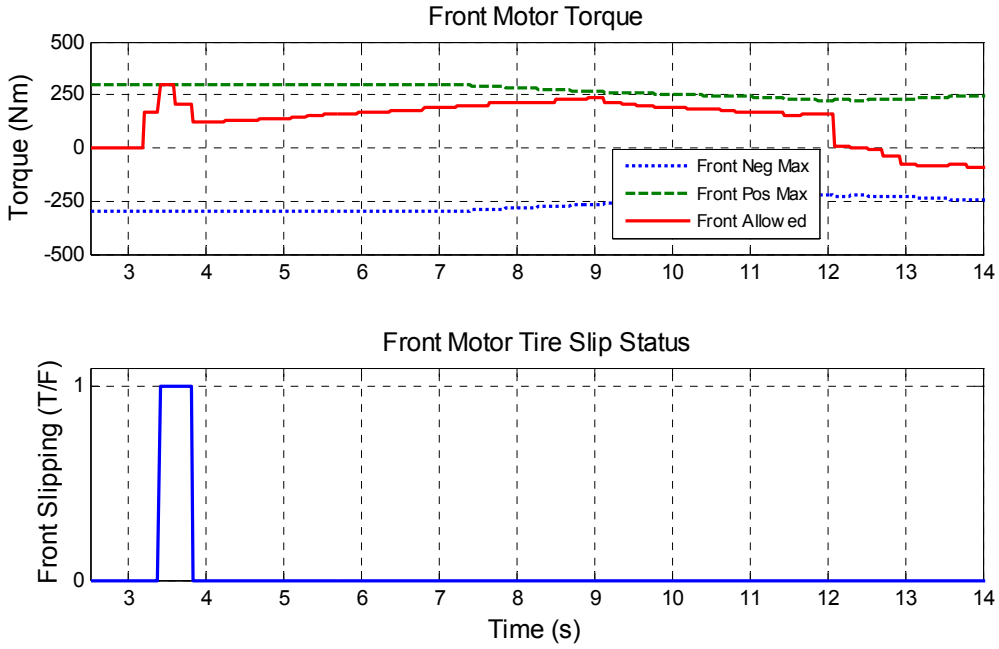

Figure D.10 Comparison between front motor torque request and slip detection for the front wheels with R_r = 1 ms.

The front TCS activates first, as seen in Fig. D.10, but as the vehicle begins to speed up, the rear TCS activates just as the front TCS deactivates. This can be seen by comparing Fig. D.10 to Fig. D.9. The front TCS deactivates because the front wheels complete the transition from the reduced traction zone to the full traction zone, and thus the wheels stop slipping. As the torque is reapplied to the front motor, the vehicle begins to accelerate, which causes the rear wheels to slip due to the large amount of torque that is still applied to the rear wheels during the increased longitudinal acceleration. The rear TCS mitigates this slip by reducing the rear torque request until the wheels catch again, as seen in Fig. D.10.

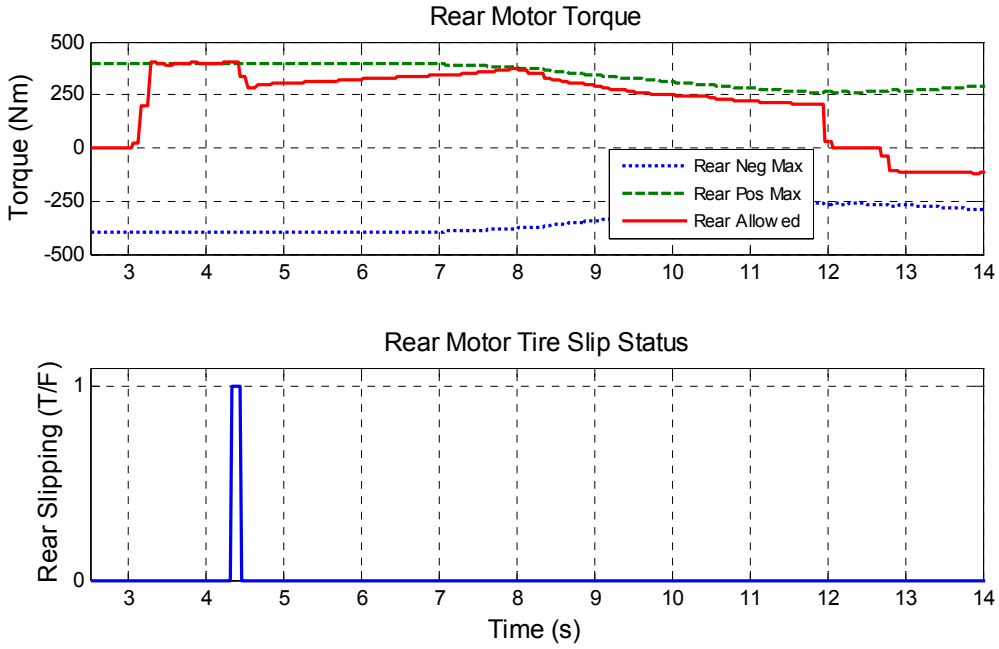

Figure D.11 Comparison between rear motor torque request and slip detection for the rear wheels with R_r = 1 ms.